Geostrophic Currents in the northern Nordic Seas from a Combination of Multi-Mission Satellite Altimetry and Ocean Modeling

Felix L. Müller[1], Denise Dettmering[1], Claudia Wekerle[2], Christian Schwatke[1], Marcello Passaro[1], Wolfgang Bosch[1], and Florian Seitz[1]

[1]Deutsches Geodätisches Forschungsinstitut, Technische Universität München, Arcisstraße 21, 80333 Munich, Germany
[2]Climate Dynamics, Alfred Wegener Institute, Helmholtz Centre for Polar and Marine Research, Bussestraße 24, 27570 Bremerhaven, Germany

Correspondence: Felix L. Müller (felix-lucian.mueller@tum.de)

Abstract.

A deeper knowledge about geostrophic ocean surface currents in the northern Nordic Seas supports the understanding of ocean dynamics in an area affected by sea ice and rapidly changing environmental conditions. Monitoring these areas by satellite altimetry results in a fragmented and irregularly distributed data sampling and prevents the computation of homogeneous and highly resolved spatio-temporal datasets. In order to overcome this problem, an ocean model is used to fill in data when altimetry observations are missing.

The present study provides a novel dataset based on a combination of along-track satellite altimetry derived dynamic ocean topography (DOT) elevations and simulated differential water heights (DWH) from the Finite Element Sea ice Ocean Model (FESOM) RJ: version 1.4. This innovative dataset differs from classical assimilation methods because it substitutes altimetry data with the model output, when altimetry fails or is not available.

The combination approach is mainly based on a Principal Component Analysis (PCA) after reducing both quantities by their constant and seasonal signals. In the main step, the most dominant spatial patterns of the modeled differential water heights as provided by the PCA are linked with the temporal variability of the estimated DOT from altimetry by performing a Principal Component Synthesis (PCS). After the combination, the RJ: ~~by altimetry obtained~~ annual signal RJ: obtained by altimetry and a constant offset are re-added in order to reference the final data product to the altimetry height level. Surface currents are computed by applying the geostrophic flow equations to the combined topography. The resulting final product is characterized by the spatial resolution of the ocean model around 1 km and the temporal variability of the altimetry along-track derived DOT heights.

The combined DOT is compared to an independent DOT product resulting in a positive correlation of about 80% to provide more detailed information about short periodic and finer spatial structures. The derived geostrophic velocity components are evaluated by in-situ surface drifter observations. Summarizing all drifter observations in equal-sized bins and comparing the velocity components shows good agreement in spatial patterns, magnitude and flow direction. Mean differences of 0.004 m/s in the zonal and 0.02 m/s in the meridional component are observed. A direct pointwise comparison between the RJ: ~~drifter trajectories~~

~~and to the drifter location interpolated combined geostrophic velocity components~~combined geostrophic velocity components interpolated onto the drifter locations indicates that about 94% of all residuals are smaller than 0.15 m/s.

The dataset is able to provide surface circulation information within the sea ice area and can be used to support a deeper comprehension of ocean currents in the northern Nordic Seas affected by rapid environmental changes in the 1995-2012 time period. The data is available at https://doi.pangaea.de/10.1594/PANGAEA.900691 (Müller et al. (2019)).

1 Introduction

Water masses flowing northwards and southwards through the Greenland Sea and Fram Strait represent the major pathways of the bidirectional water exchange between the Arctic Ocean and the Global Conveyor belt. Most of the water masses are transported via the northwards flowing West Spitsbergen Current (WSC) and the southwards flowing East Greenland Current (EGC). More than 60% of the total water transport is based on geostrophic movements, caused for example by water density and sea level elevation variations (Rudels, 2012).

Geostrophic currents (GC) can be directly derived from measurements of the dynamic ocean topography (DOT) with respect to the Earth's gravity field, rotation and the Coriolis force involved. In contrast to hydrographic pressure, temperature and salinity observations, collected by irregularly distributed in-situ data (e.g. ARGO floats or ship based measurements), satellite altimetry is the only possibility to obtain spatially and temporally homogeneous information about the global geostrophic circulation. In-situ sampling platforms can deliver high-resolution measurements, but in polar regions their availability is limited, due to a sparse spatial coverage and challenging environmental conditions. However, especially in sea ice areas, even RJ: ~~by altimetry derived geostrophic ocean currents~~geostrophic ocean currents derived by altimetry suffer from irregular sampling and data gaps. Furthermore, the generation of a dataset requires some sort of interpolation or gridding techniques, which cause smoothing effects and a coarser spatio-temporal resolution. Moreover, in open ocean regions, beyond the sea ice edge, the spatial coverage of altimetry data is sparse, due to the along-track acquisition geometry with constant and fixed orbit patterns. Hence, studies are limited to long-term means (e.g. Farrell et al. (2012)) or to satellite altimetry missions dedicated to sea ice conditions (e.g. CryoSat-2; Kwok and Morison (2015) and ICESat; Kwok and Morison (2011)). Nevertheless, monthly DOT estimates have been generated and published by Armitage et al. (2016) using DOT observations derived from long-temporal satellite altimetry. Furthermore, Armitage et al. (2017) presented a dataset based on a twelve-year altimetry observation (from 2003 to 2014) of geostrophic currents at a monthly time frame on a 0.75° × 0.25° longitude-latitude regular data grid up to a latitudinal limit of 81.5°N. The authors created a dataset, which combines satellite altimetry observations from ice-covered and open ocean regions. Further public available geostrophic ocean current products based on observational data from satellite altimetry only and in combination with in-situ buoys (e.g. Rio et al. (2014)) are provided, for example, by the GlobCurrent project and by the RJ: ~~E.U. Copernicus Marine Service Information~~Copernicus Marine Environment Monitoring Service (CMEMS). However, the latter's datasets are limited to open ocean conditions.

Besides observation-based ocean circulation products, model simulations provide information RJ: ~~of~~about the ocean dynamics. RJ: In general, their resolution is much better than these of observations, however, they rely on the underlying mathematical or

physical formulations, which naturally contain simplifications and suffer from deficiencies in process descriptions. Ocean models differ in spatio-temporal resolutions, forcing model background and underlying R1: ~~mathematical functions~~mathematical formulations. Recent developments focus on so-called unstructured ocean models, allowing for locally highly refined spatial resolutions (Danilov (2013)), while keeping a coarser resolution in other regions of the Earth (e.g. R1: ~~FESOM~~Finite Element Sea ice Ocean Model, Wang et al. (2014) or ~~MPAS~~Model for Prediction Across Scale Ocean model (MPAS-Ocean), Ringler et al. (2013)). One of the unstructured models is the Finite Element Sea ice Ocean Model R1: version 1.4 (FESOMv1.4) R1: described by Wang et al. (2014). R1: In the following text FESOMv1.4 is abbreviated by FESOM.

For the northern Nordic Seas, an eddy-resolving configuration has been developed, enabling the simulation of small-scale eddies down to 1 km (Wekerle et al. (2017)). Besides total ocean current velocities including wind-driven and geostrophic components, FESOM includes sea surface heights with respect to the bottom ocean topography, which can be also seen as an estimation of the dynamic ocean topography. Applying the gradient ~~of~~to these differential water elevations leads to the computation of simulated geostrophic currents. In contrast to observational based data, models show consistent spatio-temporal resolutions and enable investigations of ocean surface currents under the sea ice layer. However, they are limited to a fixed defined mathematical background and function as an assumption to the reality.

The current publication aims to present an innovative combined data product, based on the advantages of both, simulated and observed datasets. In contrast to other commonly used datasets or assimilation methods, the introduced product is mainly focused on the observational side by filling in modeled DOT elevations, where altimetry data is missing or corrupted. Several investigations and consistency checks have been made by Müller et al. (2019) concluding with a good agreement of simulated and observed DOT in terms of the most dominant seasonal signals and spatial patterns aiming at a combination of the temporal variability provided by altimetry along-track derived DOT elevations with simulated spatio-temporal homogeneous DOT heights of the model. The combined dataset obtained is characterized by the spatial homogeneous resolution of the model and the temporal variability of altimetry derived DOT elevations. This enables further ~~in space and time consistent~~ studies of geostrophic surface currents in sea ice regions consistent in space and time and may help to deepen the knowledge about polar ocean current dynamics.

The dataset is based on a combination of multi-mission satellite altimetry data from the ESA missions Envisat as well as ERS-2 and the eddy-resolving model, FESOM R1: version 1.4 (Wang et al. (2014)), covering a period of about 17 years. The combination approach is based on the common known Principal Component Analysis (e.g. Jolliffe (2002), Preisendorfer (1988)), which is successfully applied in historic sea level analyses and reconstruction investigations (e.g. Ray and Douglas (2011), Church et al. (2004)).

The study area covers the Fram Strait region, the Greenland Sea and parts of the Norwegian Sea as well as the Barents Sea (Figure 1). The different regions are summarized by northern Nordic Seas. In geographical coordinates the investigation area is limited to -30° W to 30° E and 72° N to 82° N.

The paper is structured in four sections. First, the datasets and combination method are introduced, followed by the results. Furthermore, the combination's reliability is evaluated by comparing the obtained datasets with in-situ drifter velocities and

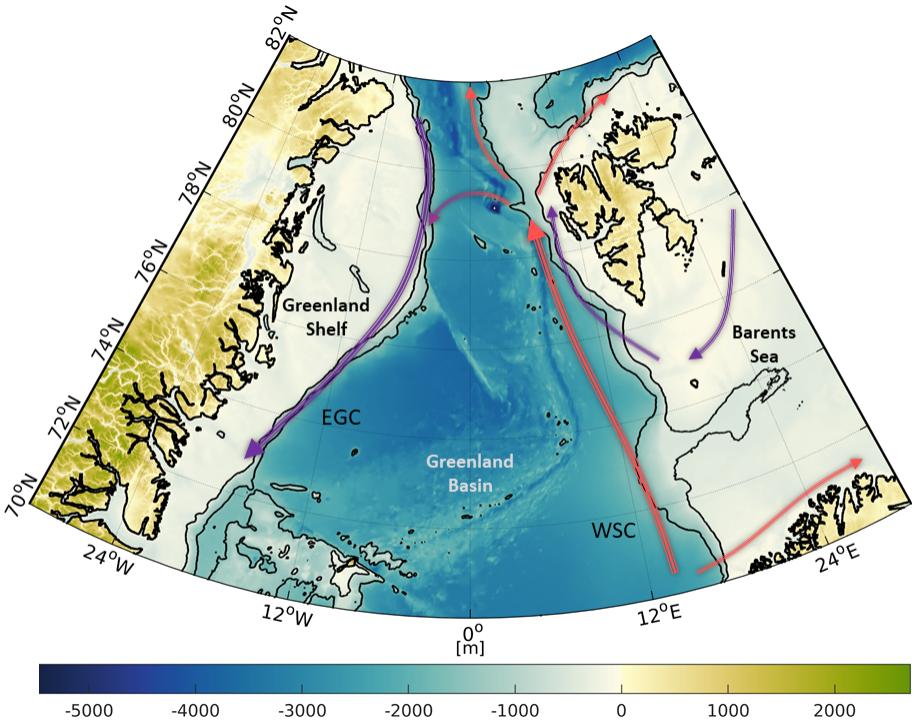

Figure 1. Bathymetry of the study area (northern Nordic Seas, Fram Strait) based on RTopo2 topography model (Schaffer et al., 2016). Major current systems (West-Spitsbergen Current, WSC; East Greenland Current, EGC) are displayed by arrows in red (inflowing Atlantic water) and blue (returning polar water). Contour lines indicate depths of -450 and -1500 meters.

independent satellite derived DOT products. The study closes with a summary and concluding remarks of the most significant aspects.

R1,R2: [New Figure 1 was added.]

2 Data

2.1 Observations: Radar altimetry data

The observational part of the combination is provided by high-frequency along-track satellite derived dynamic ocean topography data of the ESA satellites ERS-2 and Envisat. The missions cover a period of about 17 years (1995-05 - 2012-04) up to a latitudinal limit of 81.5°N. The data pre-processing ~~from~~of ERS-2 and Envisat observed ranges to derived DOT heights *R1:* ~~and~~ follow the descriptions of Müller et al. (2019). Altimetry ranges are retracked by ALES+ (Passaro et al. (2018)) and open water/sea ice discriminated by applying the method of Müller et al. (2017). The obtained sea surface heights are reduced to DOT estimates by subtracting the high resolved and *R1:* ~~combined with in-situ data~~with in-situ data combined Optimal Geoid Model for Modeling Ocean Circulation (OGMOC), developed up to a harmonic degree of 2190 (Gruber and Willberg (2018)). ALES+

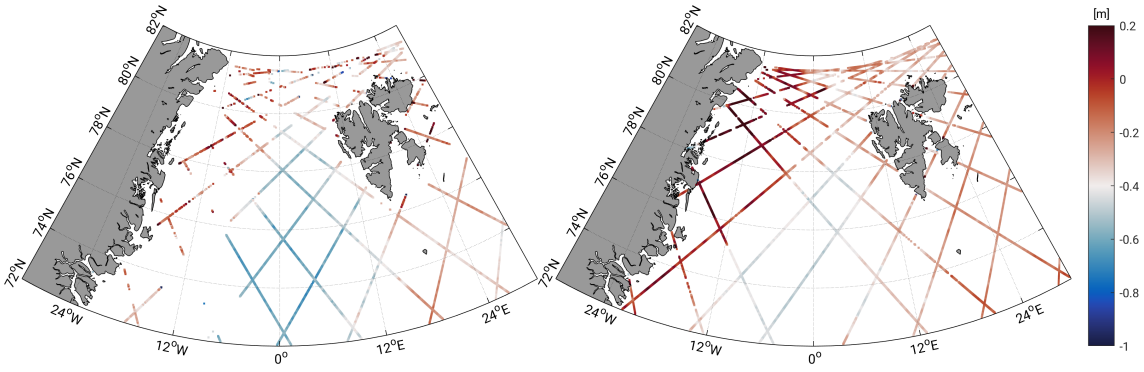

Figure 2. Exemplary pre-processed altimetry along-track DOT estimates for Envisat 3-day subcycle in March 2004 (left) and July 2006 (right), illustrating season-dependent data coverage.

has been chosen as an optimal retracking algorithm due to the ability for a consistent range estimation independent of the backscattering surface (open-ocean,lead and polynya). Coarse outliers are excluded from the dataset by filtering the sea surface heights on the basis of sea level anomalies (i.e. sea surface heights minus a mean sea surface) before transforming them to physical DOT heights. A time mean inter-mission offset is removed by taking the Envisat time series as a reference within a 6-months overlap period (2003/01 - 2003/06) considering only height observations from ice-free regions in the southern part of the investigation area. Before introducing the altimetry DOT elevations to the further processing steps, the ellipsoid referenced observation coordinates are transformed to consider the spherical Earth representation of the model.

Figure 2 shows as an example 3 days of altimetry data during the winter (March 2004) and summer (July 2006) season. In the winter, big data gaps can be noticed close to the East Greenland coast due to the presence of sea ice in contrast to summer, when most of the data is available.

2.2 Simulation: Finite Element Sea ice Ocean Model (FESOM)

The second part of the combination consists of simulated differential water heights (e.g. Figure 3) with respect to the ocean bottom topography (i.e. bathymetry). The bathymetry acts as geopotential surface, which enables a linkage to the altimetry derived DOT heights (Androsov et al. (2018)). FESOM is a global multi-resolution ocean circulation model with an included sea ice component resolving the major sea ice drift patterns. The model is based on the standard set of hydrostatic primitive equations in the Boussinesq approximation and is characterized by an unstructured triangular mesh with 47 vertical levels (Wang et al. (2014)). The horizontal resolution in the configuration used in this study reaches up to 1 km in the Fram Strait and northern Greenland Sea area and can be described as "eddy-resolving". Furthermore, the geographical model coordinates are referenced to a spherical Earth representation with a radius of 6,367.50 km. More details of the FESOM configuration can be found in Wekerle et al. (2017). The present study uses only daily differential water heights (DWH) of the surface level covering the period 2002-2009.

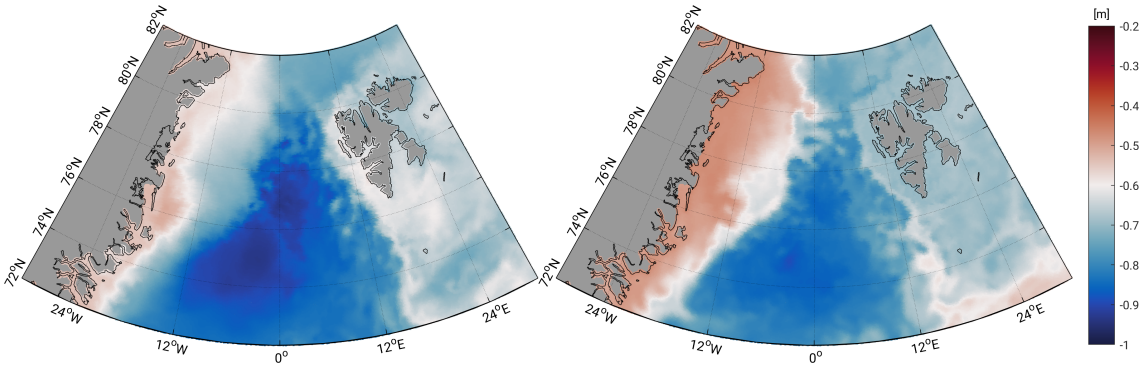

Figure 3. Exemplary differential water heights in March 2004 (left) and July 2006 (right) simulated by FESOM. R1: ~~Note the offset in comparison to Figure~~ 2. R1: Note the different scaling of colorbars in comparison to Figure 2.

2.3 Comparative datasets

For validation a comparison with externally generated absolute dynamic topography (ADT) elevations, from ADT derived geostrophic velocity components and to geostrophic ocean velocities reduced in-situ drifter observations is performed. The ADT data including geostrophic velocity components (Pujol and Mertz (2019)), provided by the R1: ~~E.U. Copernicus Marine Service Information~~ Copernicus Marine Environment Monitoring Service (CMEMS) are characterized by a daily and 1/4 degree spatial resolution and are based on multi-mission altimetry data. The ADT grids are created by adding temporal variable sea level anomalies to a mean dynamic topography and cover the complete time period of the developed datasets. However, no ADT and current data are available in sea ice areas, which limits the comparison to ice-free regions and seasons.

Further interpolated surface drifter trajectories from CMEMS (Rio and Etienne (2018)) with a 6-hour interval are used. Following the pre-processing steps of the drifting buoys, described by Rio and Etienne (2018), all surface drifters are analyzed concerning their drogue status and local wind slippage corrections. Besides geostrophic velocities, drifter observations include a-geostrophic movements (e.g. Ekman currents, Stokes drift, inertial oscillations, local wind effects, etc.). Hence, the drifter data R1: ~~must be corrected enabling~~ must be corrected in order to enable a comparison with satellite altimetry and simulated derived geostrophic currents. Local wind corrections, also provided by CMEMS (Rio and Etienne (2018)), are directly subtracted from the drifter velocities, considering the drogue status. The Ekman current is taken from global grids providing velocities at 15m depth (drogue on) and at the surface (drogue off) level. The computation of the Ekman fields follows the explanations and processing scheme of Rio and Hernandez (2003) and Rio et al. (2014). The 3-hourly available Ekman grids are downloaded from the GlobCurrent data repository and have a spatial resolution of 1/4 degrees and a global coverage. However, grid nodes north of 78.875°N are not defined, which limits the comparison to central parts of the Greenland Sea and neglects the Fram Strait area. The Ekman velocities are interpolated to the drifter positions and subtracted from the drifting buoys velocity by taking the drogue status into account. The Stokes drift is provided globally (Rascle and Ardhuin (2013) distributed by GlobCurrent) and applied only to undrogued surface drifter data in the same way like the Ekman fields (Rio et al., 2014).

Following the suggestions of Andersson et al. (2011), the Ekman and Stokes drift reduced drifter velocities are low-pass filtered by a 25-hour cutoff, two-point Butterworth filter to remove tidal and inertial oscillations. Furthermore, drifters showing observations with time gaps of more than 1 day are filtered separately (Andersson et al. (2011)).

Most of the drifter buoys observations are collected in ice-free regions affected by currents (see Figure A1). Analyzing the geostrophic amplitudes and phases, the major pathway and stream velocity of the West Spitsbergen Current is clearly identified, in contrast to the East Greenland Current, which is mostly covered by sea ice. Due to high variability, most of the drifter data can be found in the West Spitsbergen region and in the southern parts, where Atlantic water enters the Greenland Sea. Most of the drifting buoys are carried through the Fram Strait or enter the Barents Sea. Only a few drifter buoys turn around and follow the East Greenland Current. Furthermore, smaller eddies in the central Greenland Sea can be observed. In this study, nearly 70,000 in-situ observations are available, of which 63% are characterized by a drogue on status. The number of drifter measurements strongly increases between 2007 and 2012. However, nearly no data can be used between 2000 and 2006. Nevertheless, a validation of the ERS-2 data products is possible between 1995 and 2000.

3 Method

In order to generate a combined spatio-temporal consistent dataset based on irregular distributed altimetry observations, it is necessary to connect the along-track derived DOT estimates with a spatially consistent modeled DOT representation to fill the observation gaps. The following chapter describes briefly the combination of along-track DOT heights with the modeled water level, while keeping the spatial height reference of the altimetry observations.

The combination is mainly based on a Principal Component Analysis (PCA) transferring the method of historic sea level reconstruction (e.g. Church et al. (2004), Ray and Douglas (2011)) to the present purpose. Altimetry observed along-track DOT heights represent the temporal DOT variability, whereas the spatial signal is provided by FESOM. Figure 4 highlights the interrelationship of the datasets and gives an overview over the main processing chain. The individual work steps are described chronologically. The output of the processing steps are combined geostrophic currents (cGC) and dynamic ocean topography (cDOT) data representing the temporal variability of the altimetry measurements and the spatial homogeneity of the ocean model.

3.1 Data pre-processing

The input of the data production chain are along-track DOT elevations and daily simulated finite element formulated differential water heights (DWH). In order to establish an equal combination basis, both datasets are treated equally. First, they are reduced by their time mean offsets and the most dominant seasonal (i.e. annual) signal (Müller et al. (2019)).

In a second step, the reduced FESOM grids are introduced to a PCA in order to decompose them in a linearly uncorrelated, temporal part (i.e principal components) describing the temporal evolution, and in empirical orthogonal functions (EOF) identifying most dominant spatial structures of the time series. They are sorted in a decreasing order with respect to their contribution to the total signal variance. In order to reconstruct the original signal, the principal components and the corresponding EOFs

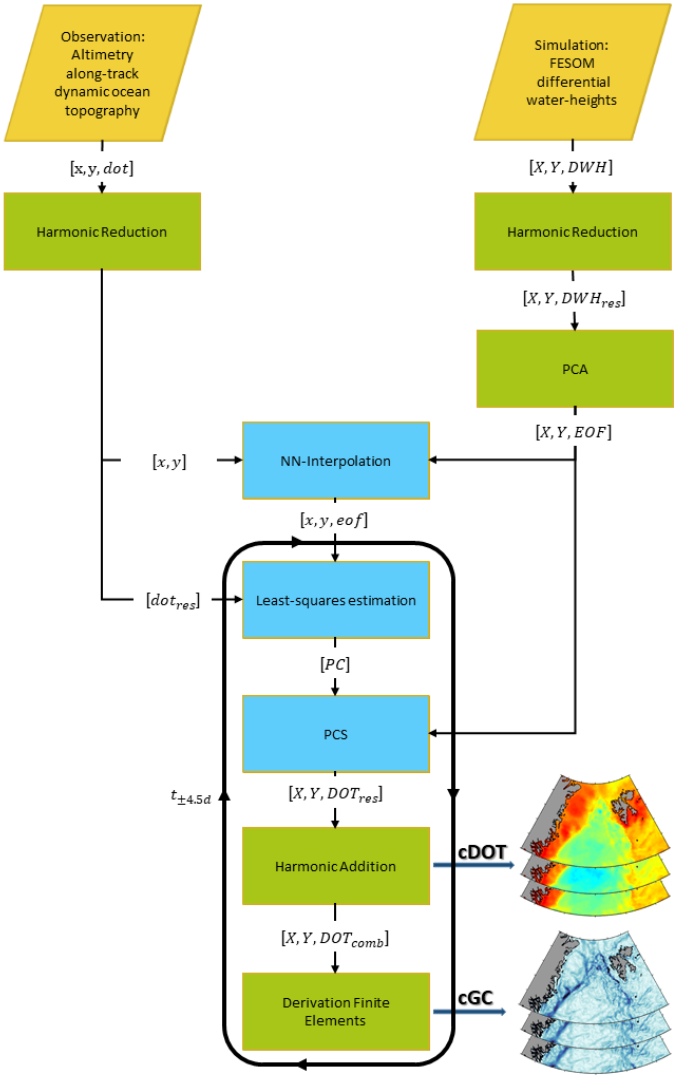

Figure 4. [Old version:]Flow chart of combined dynamic ocean topography (cDOT) and geostrophic currents (cGC) product, based on harmonic reduction, nearest-neighbor interpolation (NN-Interpolation), principal component analysis (PCA) and synthesis (PCS). Light blue indicates the combination and green auxiliary processing steps. The data sources are highlighted in yellow and pink. Data labeled in capitals indicate a grid and small letters a representation on ground tracks. Indices describe simulated (sim), observed (obs), combined ($comb$) and by annual signal and constant offset reduced (res) datasets. $t_{\pm 4.5d}$ represents the 9-day time span of used altimetry observations. [New Verssion:] Main processing chain for the generation of combined ocean topography (cDOT) and geostrophic currents (cGC) showing the main processing steps, i.e. the combination (in light blue) and auxiliary steps (in green). The necessary input data are highlighted in orange. Upper case coordinates (X, Y) are grid coordinates whereas lower case coordinates (x, y) are on the satellites' tracks. The same holds for the datasets: data labeled in capitals are given as a grid and small letters represents on along-track quantities. Index $comb$ stands for combined products, res are residual products, reduced by annual signal and constant offset. For dataset abbreviations see manuscript text.

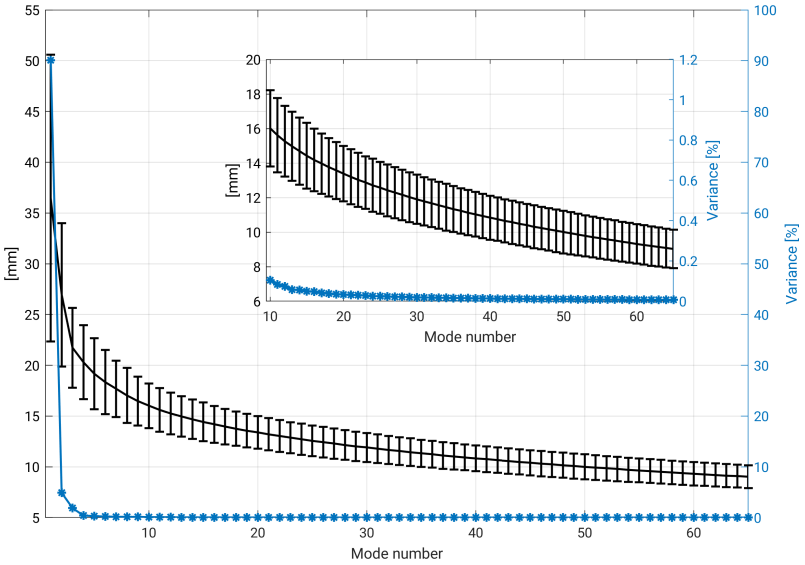

Figure 5. Percentage of variance (blue) and daily averaged root mean square error (black) including standard deviation of FESOM original data and reconstructed signal for 65 Modes of Principal Component Synthesis. For better overview, Modes 10-65 are zoomed in.

have to be multiplied and summed up. The product of one combination pair is called Mode. This inverse process of PCA is also called Principal Component Synthesis (PCS). Not necessarily PCS is used to reconstruct always the full signal, however the approach can be also limited to a certain number of retaining Modes, representing a significant percentage of the total signal. Mathematical and functional relations are explained in Jolliffe (2002). In order to determine the number of the most significant EOFs, the root mean square error (RMSE) is computed for comparing the original FESOM DWH and the reconstructed signal. The RMSE is computed by (Barnston (1992)):

$$RMSE(t) = \sqrt{\overline{(l_t - r_t)^2}} \tag{1}$$

where l substitutes the original FESOM DWH and r the reconstructed grids of the day t, where the overbar is computed over all grid nodes. Figure 5 shows the evolution of the temporal amount of variance and the temporal averaged RMSE with respect to the individual number of Modes. RI: ~~It is decided to use 50 Modes resulting in an RMSE of about 10 mm and a summed variance of more than 99%~~It is decided to use a RMSE threshold of 10mm, corresponding to 50 Modes and a summed variance of more than 99%. In the following processing steps, only the spatial signals (i.e. EOFs) of FESOM are used. In contrast, the principal components, describing the temporal evolution of the different modes, are neglected.

3.2 Combination

The combination step links the pre-processed along-track DOT heights with the most significant spatial pattern obtained from the PCA of the FESOM differential water heights. The processing is based on a daily temporal resolution, including 9 days

of radar altimetry data for each time step. The time steps are referred to the mean of a 9-day time span (i.e. $t_{\pm 4.5d}$). The combined DOT heights (cDOT) can be represented by a linear combination of n combined estimated principal components and the obtained EOF grids from FESOM. The functional relation of the PCS is described in Equation 2:

$$cDOT_{res}(X,Y,t) = \sum_{i=1}^{n} PC_i(t) \cdot EOF_i(X,Y) \tag{2}$$

where n corresponds to the number of significant principal components and empirical orthogonal functions. PC_i substitutes the n unknown combined principal components and $EOF_i(X,Y)$ the n most dominant spatial pattern on the FESOM grid (see sec. 3.1).

The principal components (PC_i) are estimated by fitting the model EOFs to the altimetry derived DOT elevations dot_{res}. Therefore, the EOF grids are interpolated to the observation coordinates based on [R2: ~~NN-Interpolation~~nearest-neighbor interpolation (NN-Interpolation)] resulting in along-track sampled empirical orthogonal functions ($eof_i(x,y)$). The solution for PC_i is then given by applying the least squares method (e.g. Koch (1999)) to Equation 3:

$$dot_{res}(x,y,t_{\pm 4.5d}) = \sum_{i=1}^{n} PC_i(t) \cdot eof_i(x,y) \tag{3}$$

where $dot_{res}(x,y,t_{\pm 4.5d})$ includes all altimetry derived DOT heights within ± 4.5 days and $eof_i(x,y)$ the corresponding along-track interpolated modeled EOFs. The result are n time series of combined principal components.

Furthermore, a Gaussian weighting, which considers uncertainties in the altimetry DOT heights due to the presence of sea ice, is introduced to the least squares process. The individual weights are defined by using an external sea ice concentration from the National Snow and Ice Data Center (NSIDC, Fetterer et al. (2017)) interpolated [R1: via nearest-neighbor interpolation] to the observation coordinates considering an enhanced error budget of altimetry range estimations, due to noisier observations ~~taken into account~~ within the sea ice area. In a last step, the estimated principal components are introduced to the PCS (Equation 2) in order to construct a combined DOT solution ($cDOT_{res}(X,Y,t)$). The individual combination steps are outlined in Figure 6 and are briefly summarized in chronological order as follows:

1. Separation of reduced FESOM DWH into most dominant spatial patterns (EOF) and time series of principal components applying PCA. However, the principal components obtained are not used but neglected, since new principal components are estimated from altimetry derived DOT and most dominant spatial patterns (EOF) of FESOM in the further combination steps.

2. Nearest-neighbor interpolation of EOF to altimetry along-track observations (x,y) obtaining profiled eof.

3. Least squares estimation of combined principal components (PC_i) by solving Equation 3 based on altimetry DOT observations (dot_{res}) and interpolated empirical orthogonal functions (eof).

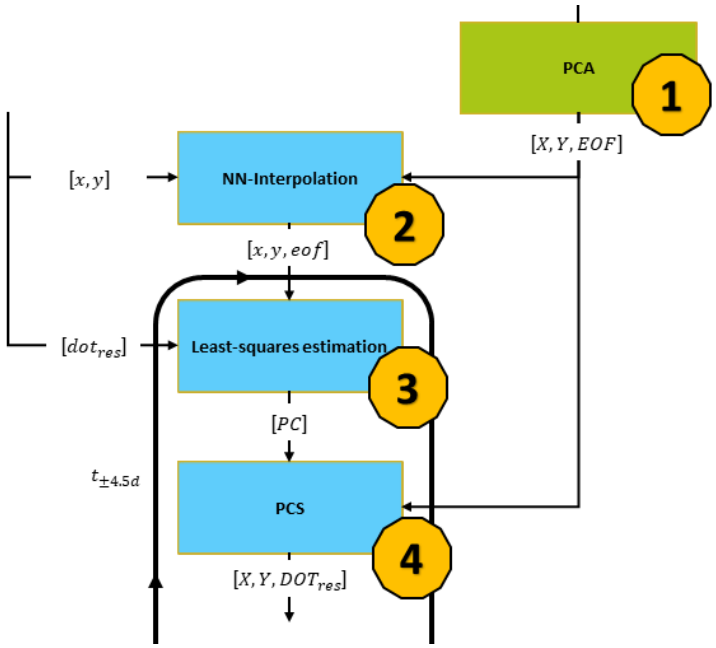

Figure 6. Subset of Figure 4 outlining combination steps. Numbers indicate the chronological order of the individual processing steps.

4. Application of Equation 2 to obtain the combined DOT ($cDOT_{res}$) dataset in the FESOM grid (X, Y) based on PC_i (step 3) and EOF (step 1).[R2:] Furthermore, an outlier detection based on an accuracy determination of the combined principal components is performed to reject erroneous combination estimations.

3.3 Data generation

In order to reconstruct the full signal and to rescale the combined heights to the altimetry height reference, the previous subtracted altimetry time mean offset and annual signal are re-added (Sect. 3.1). In the next step, combined geostrophic currents (cGC) are obtained by computing the zonal (u_g) and meridional (v_g) geostrophic velocity components at the surface, given by Equation 4:

$$u_g = -\frac{g}{f}\frac{\partial h}{\partial y}$$
$$v_g = \frac{g}{f}\frac{\partial h}{\partial x} \tag{4}$$

where g is the acceleration of gravity ($9.832\ \frac{m}{s^2}$), $f = 2\Omega \sin\phi$ the Coriolis force, ϕ the latitude and Ω the Earth's rotation rate. ∂h denotes the horizontal gradient in x and y direction of cDOT height h. The derivatives $\frac{\partial h}{\partial y}$ and $\frac{\partial h}{\partial x}$ are solved based on the finite element method (see Appendix B) which prevents further smoothing effects[R1:], since no re-gridding to a regular grid

is necessary. Furthermore, the geostrophic absolute velocity (A_g), phase ϕ_g and eddy kinetic energy (EKE) can be computed by applying Equation 5.

$$\begin{aligned} A_g &= \sqrt{u_g^2 + v_g^2} \quad \phi_g = \arctan \frac{v_g}{u_g} \\ EKE &= \frac{1}{2}((u_g(t) - \overline{u_g})^2 + (v_g(t) - \overline{v_g})^2) \end{aligned} \tag{5}$$

where t substitutes the velocity at a certain time and the overbar indicates the mean velocity for a defined time period (e.g. quarterly).

4 Datasets

The combined DOT and geostrophic current velocity fields R2: ~~contain~~are based on DOT heights derived from satellite altimetry and simulated differential water heights from FESOM (Müller et al. (2019)). The dataset spans a time period from mid-May 1995 to early April 2012 and covers the investigation area of the northern Nordic Seas limited to -30° W - 30° E and 72° N - 82° N. The dataset is saved in NetCDF format. As a result of the combination process, the processed grids are stored in a daily temporal and unstructured spatial resolution with local refinements up to 1 km. Missing days in the dataset due to longer periods of missing altimetry observations R2: and unreliable combined principal components are possible. R2: ~~Furthermore, an outlier detection based on the accuracy of the computed combined principal components is performed rejecting erroneous combination estimations.~~ The data product is given in units of meters in case of DOT and in m/s for the geostrophic components.

Figure 7 illustrates quarterly averaged daily combined DOT heights and derived geostrophic components expressed in velocity and azimuth. All meshes show the same spatial resolution with local refinements in the central Greenland Sea and Fram Strait region (approx. 1 km) and implicate the finite element structure of the input model. The three-monthly averaged cDOT fields vary by circa 1 m across the northern Nordic Seas with maximum variations in the winter months. Furthermore, the anti-phase relationship in the annual oscillation (Bulczak et al. (2015)) between the deep basins and the shelf areas in winter and summer can be seen. The derived geostrophic components show a strong meandering West Spitsbergen Current and a more clear flow structure in the East Greenland Current.

5 Comparison with external datasets

The produced datasets are compared ~~with~~to independent datasets providing daily sampled DOT heights and observations of surface drifter buoys. However, it must be noted that the comparison is challenging since no dataset can be used as ground truth in the whole ~~area of study~~study area.

In order to follow a comparison with in-situ observations, the combined geostrophic components are spatio-temporally interpolated to surface drifter locations. This enables the analyses of differences between geostrophic currents from observations and from the derived combined product. Therefore, the combination procedure is applied to the drifter epochs. This is done by

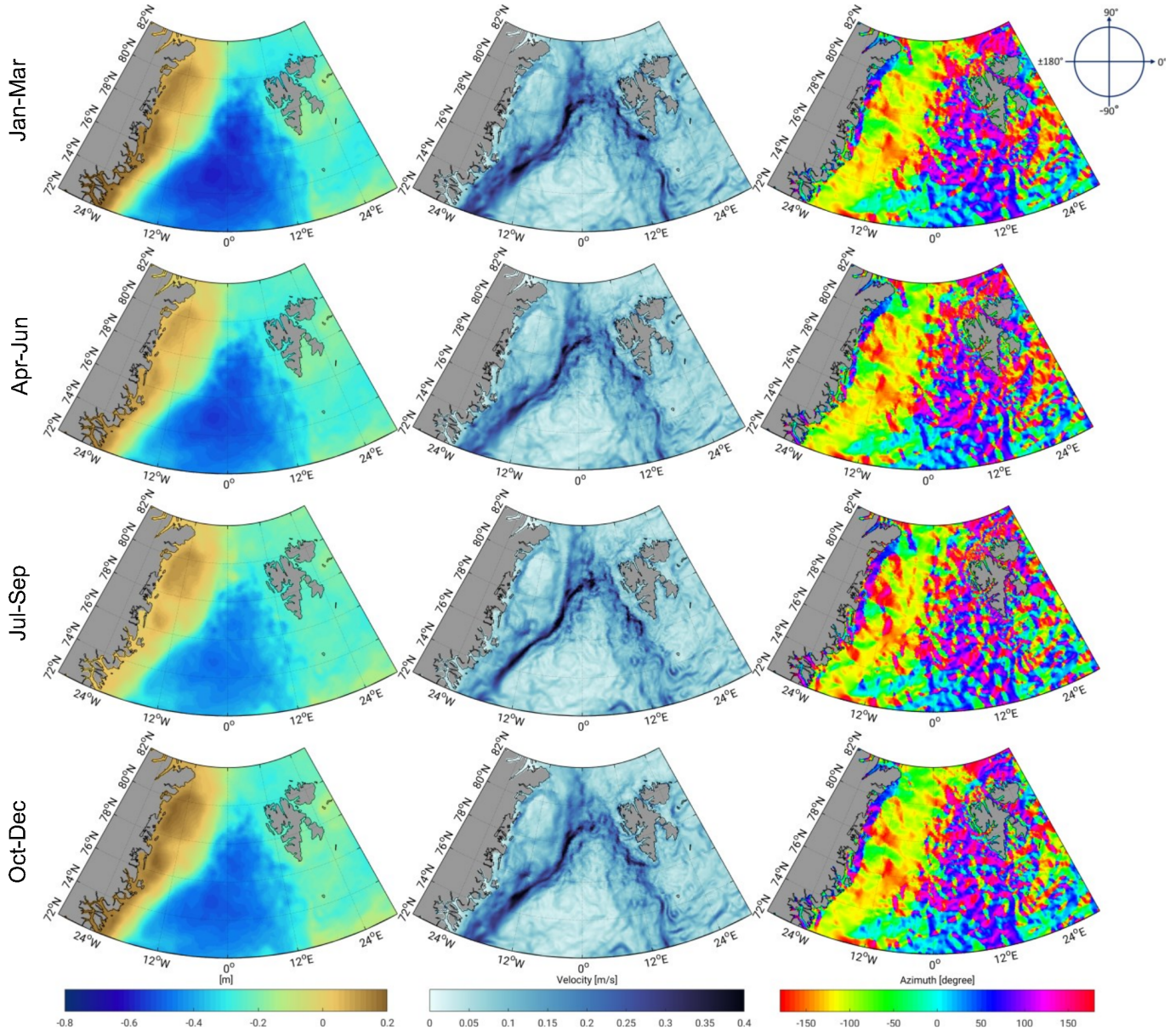

Figure 7. Three-monthly averaged combined DOT heights (left), absolute geostrophic velocities (middle) and flow direction (right) from 1995 to 2012.

interpolating the estimated combined principal components linearly to the drifter times followed by a PCS (eq. 2) and a spatial nearest-neighbor interpolation to the drifter location. The result are combined DOT heights at the drifter observation time and location. In order to compare with the geostrophic drifter measurements, the cDOT heights are transformed to geostrophic velocities (sec. 3.3). Following Andersson et al. (2011), the drifter observations are grouped into 2°x 1° longitude latitude boxes. In order to perform statistically reliable analyses, only bins with at least 2 different surface drifters and 50 observations are used (Andersson et al. (2011)).

Figure 8 displays in time-averaged u and v components of the drifter observations (first row) and the combined geostrophic currents (middle row). The differences (bottom row) agree well with spatial patterns of the velocity components (i.e. drifter - combination). The East Greenland and West Spitsbergen Current are resolved by both datasets in both velocity components. The drifter and the cGC describe the same amplitude and flow direction in most of the bins. However, the v component shows bigger differences than the zonal component, caused mainly by a higher variability due to the primarily meridional flow direction of the currents in this area. Good agreement to the drifter data is shown by slight mean differences of 0.004 m/s ± 0.02 m/s in the zonal (u) and 0.01 m/s± 0.04 m/s in the meridional (v) component.

R2: ~~Computing directly the RMSE based on the individual trajectories between the drifter and combined velocity components for each drifter,~~ When computing the RMSE between the measured geostrophic velocities and the combined velocities based on the individual trajectories for each drifter, a mean of 0.127 m/s± 0.034 m/s in case of the u-velocity and 0.132 m/s± 0.039 m/s for the v-velocity are obtained. Moreover, the RMSE may reach 0.225 m/s for u and 0.232 m/s for v. Higher RMSE values can be found in regions with strong current activity (e.g. WSC).

Figure 9 shows the RMSE distribution of absolute velocity (Equation 5) for the period 1995-2012 (blue curve). In addition, the same quantity derived based on the altimetry-only ADT currents is plotted in green. Both datasets are characterized by a very similar behavior. Nevertheless, the combination shows smaller residuals. 35% of the combined residuals are smaller than 0.1 m/s in contrast to 27% of the altimetry only derived geostrophic absolute velocity. In general, the results of both datasets are comparable to previous studies of the World Ocean and to Volkov and Pujol (2012) describing a maximal RMSE of around 0.2 m/s and a typical range of 0.07 m/s to 0.15 m/s for the northern Nordic Seas in both components.

Figure 10 shows daily three-monthly averaged EKE of the combined and ADT grids within the investigation period (1995-2012). The EKE results are computed by subtracting three-monthly means from the daily datasets (Equation 5). The ADT appears smoother and shows big data gaps in sea ice regions in comparison ~~with~~to the combined results. Furthermore, the combined eddy fields show finer eddy structures within the sea ice area and close to the Greenland coast. The cGC are characterized by a higher spatial resolution and more variability in current regions.

The cDOT grids are evaluated against the daily and spatial averaged time series of ADT fields. Therefore, the cDOT fields are spatially interpolated to the ADT grids. Figure 11 shows the by their mean reduced temporal evolution of both datasets. The comparison covers the full investigation period, but is spatially limited to ice-free regions. The time series indicate a positive temporal correlation of nearly 80%. Both datasets display high-frequent patterns. Compared to the stronger smoothed ADT grids with a standard deviation (std) of ± 0.04 m, the cDOT heights are characterized by a higher variability (std= ± 0.05 m) and display short periodic structures. Nevertheless, a slight offset between the time series between 1995 and 2003 of 2.5 cm

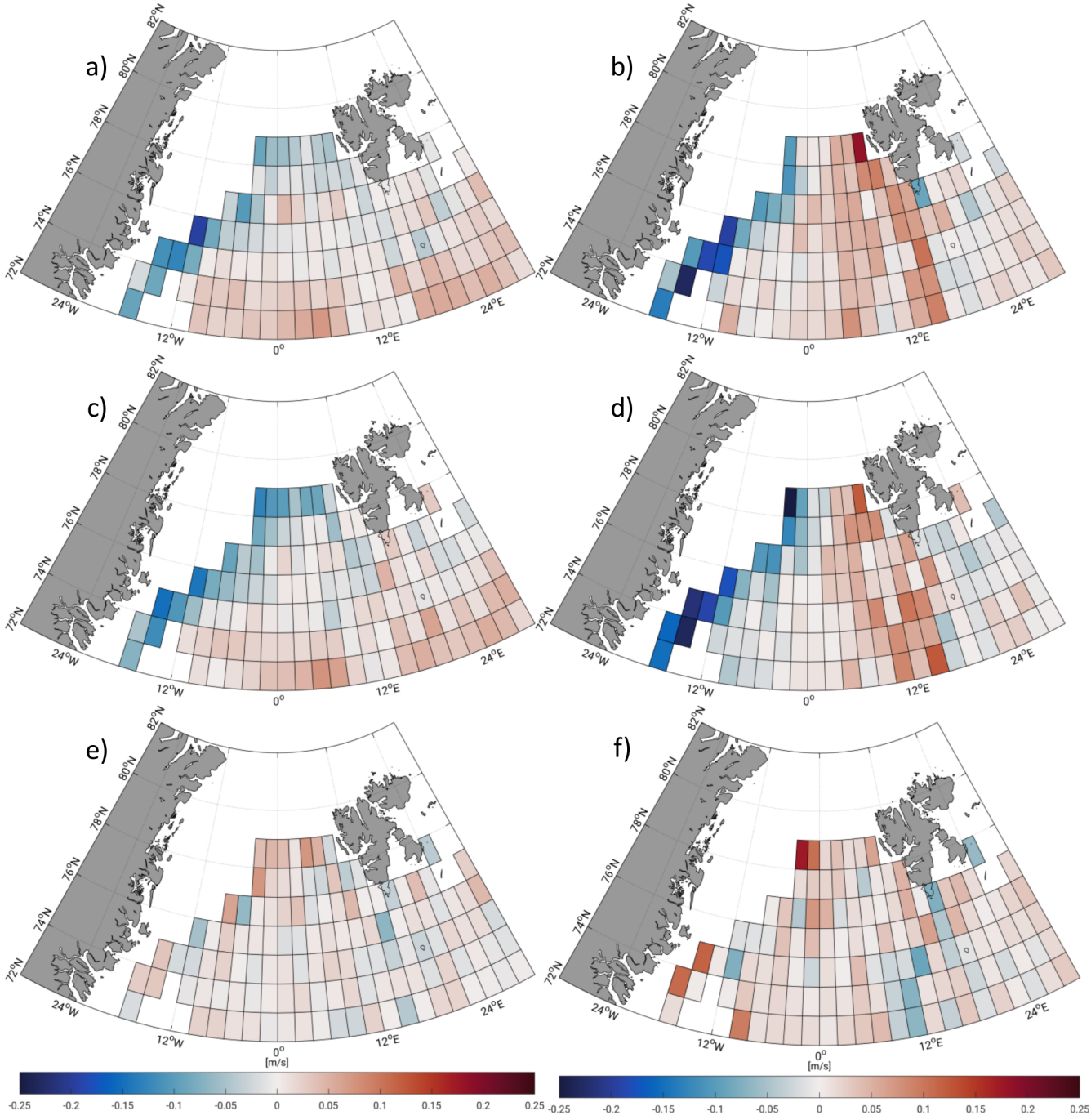

Figure 8. Temporal averaged geostrophic u (left) and v (right) components of drifter observations (a,b), combined dataset (c,d) and differences (e,f), respectively, binned in 2°x1°(lon,lat) boxes within the investigation time (1995-2012).[RJ:] ~~Please note the changed scale of the differences.~~

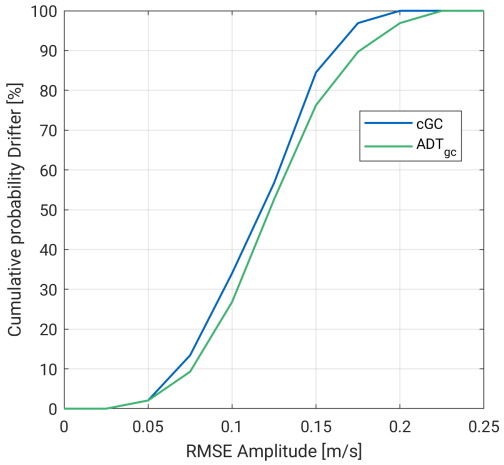

Figure 9. RMSE of geostrophic absolute velocity between drifter observations and to the trajectories interpolated combined and ADT datasets from 1995 to 2012.

and 2.0 cm between 2003 and 2012 can be observed, which might occur due to a different applied mean epoch of the ADT computation or an unconsidered bias in the retracking procedure of ERS-2 and Envisat.

6 Summary and Conclusions

The current paper presents an innovative dataset based on a combination of height observations from satellite altimetry with spatial information provided by an ocean model (FESOM). In case of altimetry data, an open water classification procedure is applied in order to exploit along-track water height measurements within the sea ice area. Furthermore, height offsets between the open ocean and the sea ice area are removed by using one single retracking algorithm.

The combination approach takes advantage of the principal component analysis, especially the separation of the model data into its most significant spatial patterns and temporal components with respect of the total variability. The 50 most dominant patterns (EOF) are used to combine them with ERS-2 and Envisat observed along-track DOT heights in order to fill in observational gaps and to enable investigations based on a homogeneous DOT representation. In detail, the spatial information from FESOM and the temporal variability from altimetry are linked. The height level of the final product is given by altimetry by re-adding the previous estimated and subtracted annual signal and constant offset, since the model height reference is not clearly defined, whereas the obtained spatial resolution is RI: ~~given~~defined by FESOM, RI: which is characterized by local refinements in ocean current active areas smaller than 1 km. The combination is computed on a daily resolution and covers a time span of 17 years (1995-2012).

Geostrophic currents are provided by computing zonal and meridional slope gradients of the finite element mesh. This allows comprehensive variability analyses of ocean currents not only in open ocean areas, but also within sea ice regions. A comparison with altimetry-only datasets shows that the combination convinces by an enhanced spatio-temporal resolution,

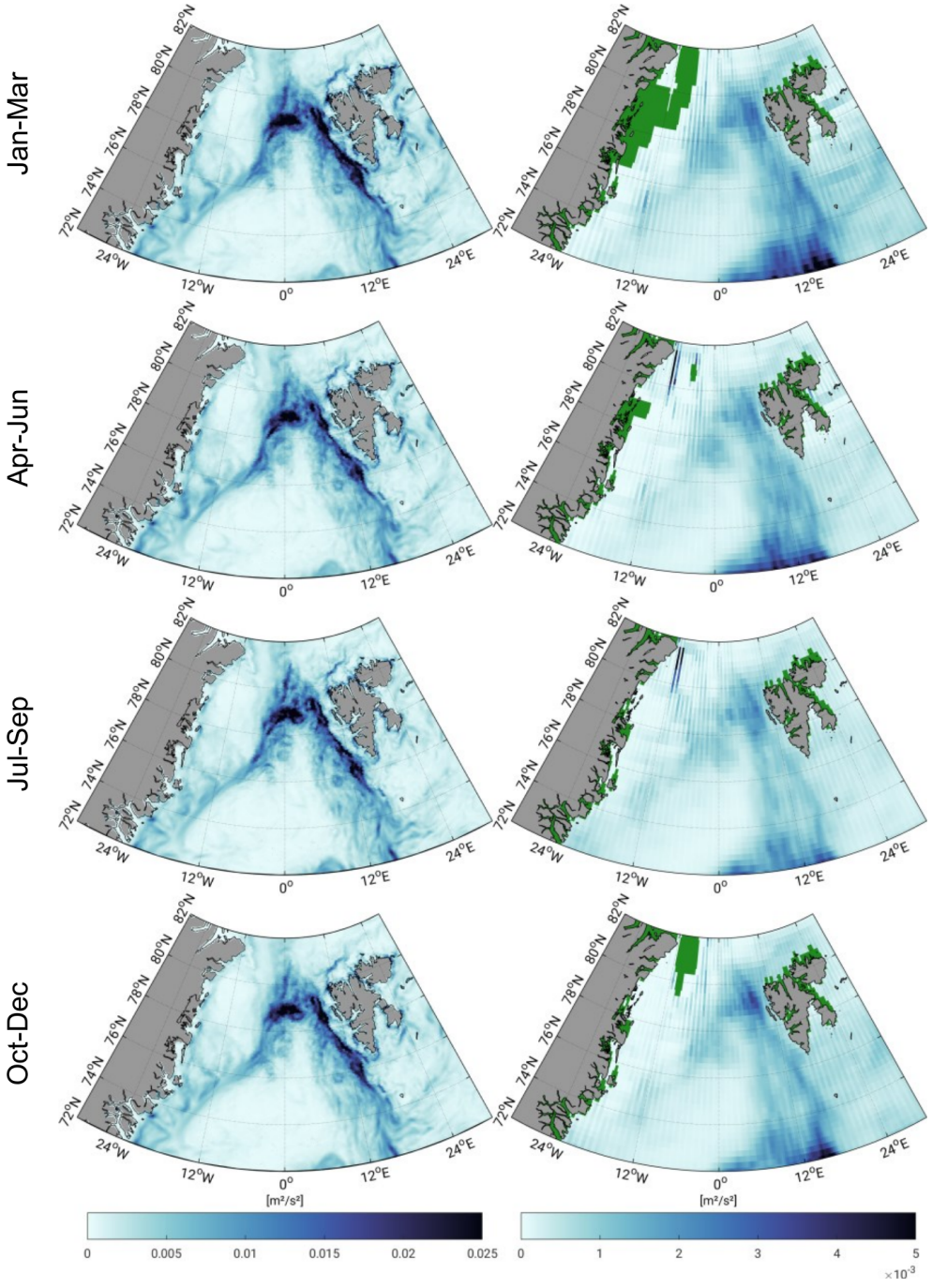

Figure 10. Three-monthly averaged geostrophic eddy kinetic energy within the FESOM period (1995-2012) for combined results (left) and ADT grids (right). Green areas indicate missing values.

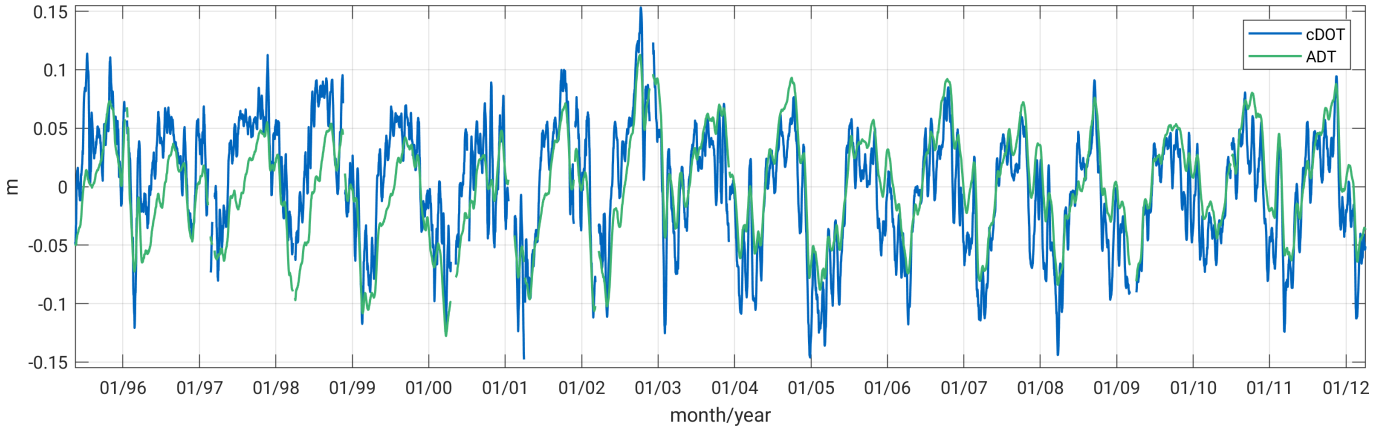

Figure 11. Zero-centered time series of daily and spatial averaged altimetry-only ADT grids and to the ADT grid nodes interpolated combined DOT (cDOT) limited to ice-free regions within 1995-2012 and the northern Nordic Seas.

displays short periodic structures and missing data gaps, especially in the regions covered by sea ice. Moreover, a positive correlation of nearly 80% in open ocean areas can be achieved.

A comparison with in-situ surface drifter measurements, although limited to ice-free regions, indicates a similar and realistic representation of ocean current patterns and meso-scale eddies in the area of both datasets under investigation. Furthermore, a good agreement in the comparison of binned surface drifter and derived combined geostrophic velocity components has been described. *RI:* ~~A comparison with the uncompressed FESOM geostrophic currents in terms of EKE displays a small improvement by the combined dataset.~~

A direct pointwise comparison for each drifter trajectory indicates a temporal RMS of the differences between the drifter velocity components and the combination of about 0.13 m/s. In general, the RMSE values obtained range from 0.05 m/s to 0.10 m/s in areas with low-flow activity and up to 0.22 m/s in regions with high current energy. Following Volkov and Pujol (2012), this velocities are comparable to previous estimates for the World Ocean.

The presented data product supports long-temporal studies of the dynamic ocean topography and the ocean current regime in polar regions affected by sea ice. Aiming at a more than 25 years covering extension of the dataset more conventional altimetry (Saral, ERS-1) as well as Delay-Doppler altimetry data (e.g. Sentinel-3A/B, CryoSat-2) will be added to the combination process in the future.

7 Data availability

The final combined dataset can be downloaded from PANGAEA, https://doi.pangaea.de/10.1594/PANGAEA.900691 (Müller et al. (2019)). Envisat (SGDR) and ERS-2 (REAPER-SGDR) altimetry data access is available from ESA (Envisat, https://doi.org/10.5270/EN1-85m0a7b, ESA (2018); ERS-2, https://earth.esa.int/web/guest/-/radar-altimeter-reaper-sensor-geophysical-data-record-sgdr, Brockley et al. (2017)). *RI:* The used FESOM data can be downloaded from PANGAEA, https://doi.org/10.1594/PANGAEA.880569 or requested from C. Wekerle (AWI). *RI:* The model

code can be downloaded from https://swrepo1.awi.de/projects/fesom [R1:] after registration. The in-situ drifter observations and ADT grids with additional parameters are available via CMEMS (drifter data, http://resources.marine.copernicus.eu/?option=com_csw&view=details&product_id=INSITU_GLO_UV_L2_REP_OBSERVATIONS_013_044, Rio and Etienne (2018); ADT, http://resources.marine.copernicus.eu/?option=com_csw&view=details&product_id=SEALEVEL_GLO_PHY_L4_REP_OBSERVATIONS_008_047, Pujol and Mertz (2019)). Data grids of the Ekman- and Stokes drift are provided by GlobCurrent http://globcurrent.ifremer.fr/products-data/data-catalogue.

Acknowledgements. The authors thank Hélène Etienne from Collecte Localisation Satellites (CLS) for supporting the study with valuable advice regarding the surface drifter data processing. The authors thank the Chair of Astronomical and Physical Geodesy, Technical University of Munich (TUM) for providing the geoid model, OGMOC. We also thank ESA for providing ERS-2 and Envisat altimetry data, CMEMS for maintaining the ADT grids as well as the surface drifter velocities and GlobCurrent for providing a-geostrophic currents (i.e. Ekman, Stokes drift). This work was mainly supported by the German Research Foundation (DFG) through grants, BO1228/13-1, DE2174/3-1 and (SPP)-1889 "Regional Sea Level Change and Society". The publication is funded by the German Research Foundation (DFG) and the Technical University of Munich (TUM) in the framework of the Open Access Publishing Program.

We thank two anonymous reviewers for their valuable comments that helped to improve the manuscript.

Author contributions. Felix L. Müller processed the combination and wrote most of the paper. Denise Dettmering supervised the present study, contributed to the manuscript writing and helped with discussions of the results. Claudia Wekerle provided the FESOM data and contributed to the manuscript writing. Christian Schwatke maintains the altimetry data base (OpenADB) at DGFI-TUM and supports with discussions. Marcello Passaro developed the retracking algorithm and helped with discussion concerning the altimetry dataset. Wolfgang Bosch initiated the study. Florian Seitz supervised the research.

Competing interests. The authors declare no conflict of interests.

Appendix A: Abbreviations and Nomenclature of altimetric and FESOM height variables

[R1:] [Please note added Appendix A]

- SSH: sea surface heights; heights with respect to a reference ellipsoid
- SLA: sea level anomalies; heights with respect to a mean sea level
- DOT: dynamic ocean topography; heights with respect to a geopotential datum (i.e. geoid)
- ADT: absolute dynamic topography; identical to DOT (nomenclature used by AVISO)

– DWH: differential water height; simulated elevations with respect to a reference defined as being identical to the geoid but without considering secular changes (e.g. self gravitation, ocean bottom topography, Glacial Isostatic Adjustment, GIA); closely related to DOT

Appendix B: Derivation of Finite-Elements in FESOM

The FESOM configuration that was used is based on a finite element formulation. Regarding the spatial discretization, the global ocean is discretized by using tetrahedral elements. These elements are constructed by first generating a surface triangular mesh (x, y). In the vertical, z-layers are used. The resulting vertical prisms are then cut into three tetrahedrals. In the finite element method, variables are approximated as linear combinations of a finite set of basis functions $\{N_i\}$. Regarding the choice of these basis functions, FESOM uses a P1-P1 discretization, meaning that piecewise linear basis functions are employed for both sea surface height η and horizontal velocity $\mathbf{u}$:

$$\eta = \sum_{i=1}^{N_{2D}} \eta_i N_i \text{ and } \mathbf{u} = \sum_{i=1}^{N_{3D}} u_i N_i,$$

where N_{2D} and N_{3D} denote the number of 2D and 3D nodes respectively. The ith basis function N_i is equal to 1 at node i and linearly vanishes to 0 within elements containing this node.

Derivatives are computed by transformation to a reference element. In 2D, we consider the reference element $\hat{K}$ defined by nodes $\hat{a}_1 = (0,0)$, $\hat{a}_2 = (1,0)$ and $\hat{a}_3 = (0,1)$. As local 2D basis functions defined on $\hat{K}$, we choose the first order polynomials

$$N_1(x,y) = 1 - x - y,\ N_2(x,y) = x \text{ and } N_3(x,y) = y,$$

with its Jacobian matrix $J_N = \begin{pmatrix} -1 & -1 \\ 1 & 0 \\ 0 & 1 \end{pmatrix}$. Any arbitrary element K in the physical domain defined by nodes a_1, a_2 and a_3 can be mapped on the reference element $\hat{K}$ by affine-linear transformation:

$$F:\ \hat{K} \to K,\ F(\hat{x}) = B\hat{x} + d,$$

with $B = (a_2 - a_1, a_3 - a_1)$ and $d = a_1$. When computing the gradient of a variable ϕ on the reference element $\hat{K}$, we obtain:

$$\nabla_{\hat{x}}\phi(x) = \nabla_{\hat{x}}\phi(F(\hat{x})) = \nabla_x\phi(F(\hat{x}))\nabla_{\hat{x}}F(\hat{x}) = \nabla_x\phi(F(\hat{x}))B,$$

Thus, the gradient in the physical domain can be expressed as:

$$\nabla_x\phi(F(\hat{x})) = \nabla_{\hat{x}}\phi(F(\hat{x}))B^{-1}.$$

We now compute the gradient of η on element K by inserting $\phi = \sum_{i=1}^{3} \eta_i N_i$ in the above equation:

$$\nabla_x\eta = \nabla_{\hat{x}} \sum_{i=1}^{3} \eta_i N_i B^{-1} = (\eta_1, \eta_2, \eta_3) J_N B^{-1}.$$

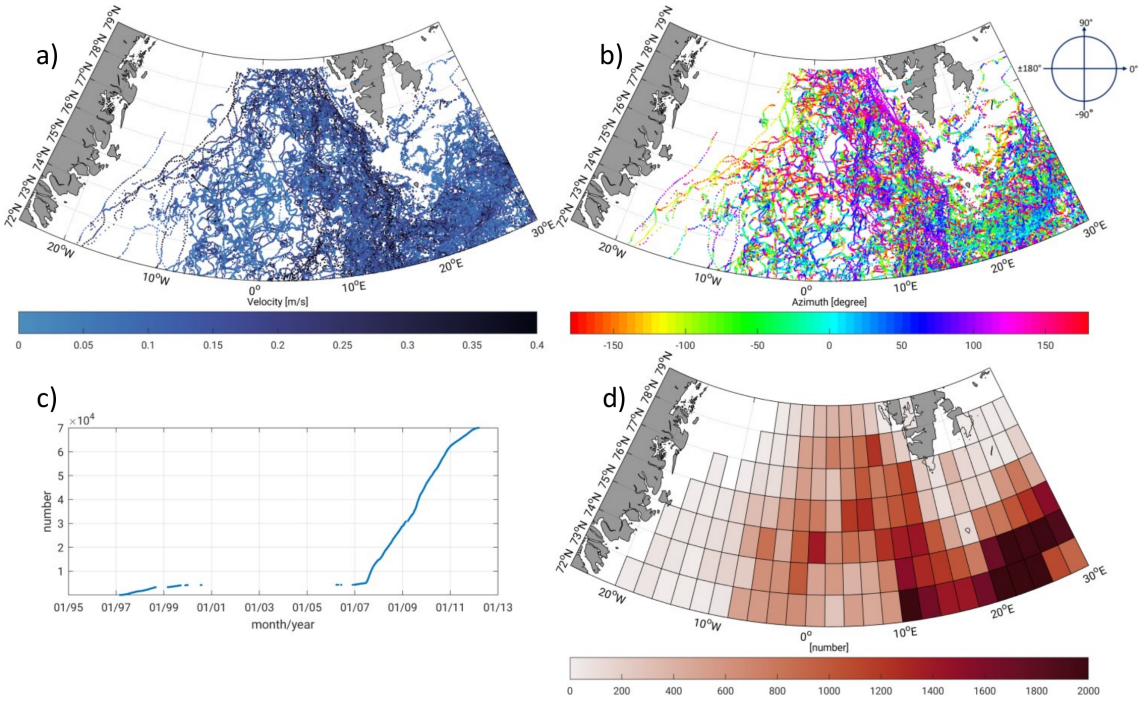

Figure A1. Amplitude (a), azimuth (b), cumulative number (c) of geostrophic surface drifter velocities and number of records in 2°x1° boxes (d) within the 1995-2012 investigation time period. Approximately 63% of the observations were obtained by an attached drogue.

References

Andersson, M., Orvik, K. A., LaCasce, J. H., Koszalka, I., and Mauritzen, C.: Variability of the Norwegian Atlantic Current and associated eddy field from surface drifters, Journal of Geophysical Research: Oceans, 116, https://doi.org/10.1029/2011JC007078, 2011.

Androsov, A., Nerger, L., Schnur, R., Schröter, J., Albertella, A., Rummel, R., Savcenko, R., Bosch, W., Skachko, S., and Danilov, S.: On the assimilation of absolute geodetic dynamic topography in a global ocean model: impact on the deep ocean state, Journal of Geodesy, https://doi.org/10.1007/s00190-018-1151-1, 2018.

Armitage, T. W. K., Bacon, S., Ridout, A. L., Thomas, S. F., Aksenov, Y., and Wingham, D. J.: Arctic sea surface height variability and change from satellite radar altimetry and GRACE, 2003–2014, Journal of Geophysical Research: Oceans, 121, 4303–4322, https://doi.org/10.1002/2015JC011579, 2016.

Armitage, T. W. K., Bacon, S., Ridout, A. L., Petty, A. A., Wolbach, S., and Tsamados, M.: Arctic Ocean surface geostrophic circulation 2003–2014, The Cryosphere, 11, 1767–1780, https://doi.org/10.5194/tc-11-1767-2017, 2017.

Barnston, A. G.: Correspondence among the Correlation, RMSE, and Heidke Forecast Verification Measures; Refinement of the Heidke Score, Weather and Forecasting, 7, 699–709, https://doi.org/10.1175/1520-0434(1992)007<0699:CATCRA>2.0.CO;2, 1992.

Brockley, D. J., Baker, S., Féménias, P., Martínez, B., Massmann, F., Otten, M., Paul, F., Picard, B., Prandi, P., Roca, M., Rudenko, S., Scharroo, R., and Visser, P.: REAPER: Reprocessing 12 Years of ERS-1 and ERS-2 Altimeters and Microwave Radiometer Data, IEEE Transactions on Geoscience and Remote Sensing, 55, 5506–5514, https://doi.org/10.1109/TGRS.2017.2709343, 2017.

Bulczak, A. I., Bacon, S., Naveira Garabato, A. C., Ridout, A., Sonnewald, M. J. P., and Laxon, S. W.: Seasonal variability of sea surface height in the coastal waters and deep basins of the Nordic Seas, Geophysical Research Letters, 42, 113–120, https://doi.org/10.1002/2014GL061796, 2014GL061796, 2015.

Church, J. A., White, N. J., Coleman, R., Lambeck, K., and Mitrovica, J. X.: Estimates of the Regional Distribution of Sea Level Rise over the 1950–2000 Period, Journal of Climate, 17, 2609–2625, https://doi.org/10.1175/1520-0442(2004)017<2609:EOTRDO>2.0.CO;2, 2004.

Danilov, S.: Ocean modeling on unstructured meshes, Ocean Modelling, 69, 195 – 210, https://doi.org/10.1016/j.ocemod.2013.05.005, 2013.

ESA: RA-2 Sensor and Geophysical Data Record - SGDR, https://doi.org/10.5270/en1-85m0a7b, 2018.

Farrell, S. L., McAdoo, D. C., Laxon, S. W., Zwally, H. J., Yi, D., Ridout, A., and Giles, K.: Mean dynamic topography of the Arctic Ocean, Geophysical Research Letters, 39, https://doi.org/10.1029/2011GL050052, 2012.

Fetterer, F., K., Knowles, W., Meier, M., Savoie, and Windnagel, A. K.: Sea Ice Index, Version 3, north, Boulder, Colorado USA. NSIDC: National Snow and Ice Data Center, https://doi.org/10.7265/N5K072F8, accessed: 2019-01-15, 2017.

Gruber, T. and Willberg, M.: Signal and Error Assessment of GOCE-based High Resolution Gravity Field Models, Journal of Geodetic Science, under review, 2018.

Jolliffe, I. T.: Principal Component Analysis, vol. 2, Springer-Verlag New York, https://doi.org/10.1007/b98835, 2002.

Koch, K.-R.: Parameter Estimation and Hypothesis Testing in Linear Models, Springer Berlin Heidelberg, https://doi.org/10.1007/978-3-662-03976-2, 1999.

Kwok, R. and Morison, J.: Dynamic topography of the ice-covered Arctic Ocean from ICESat, Geophysical Research Letters, 38, https://doi.org/10.1029/2010GL046063, 2011.

Kwok, R. and Morison, J.: Sea surface height and dynamic topography of the ice-covered oceans from CryoSat-2: 2011–2014, Journal of Geophysical Research: Oceans, 121, 674–692, https://doi.org/10.1002/2015JC011357, 2015.

Müller, F. L., Dettmering, D., Wekerle, C., Schwatke, C., Bosch, W., and Seitz, F.: Geostrophic Currents in the northern Nordic Seas - A Combined Dataset of Multi-Mission Satellite Altimetry and Ocean Modeling (data), https://doi.org/10.1594/PANGAEA.900691, https://doi.org/10.1594/PANGAEA.900691, 2019.

Müller, F. L., Wekerle, C., Dettmering, D., Passaro, M., Bosch, W., and Seitz, F.: Dynamic ocean topography of the northern Nordic seas: a comparison between satellite altimetry and ocean modeling, The Cryosphere, 13, 611–626, https://doi.org/10.5194/tc-13-611-2019, 2019.

Müller, F. L., Dettmering, D., Bosch, W., and Seitz, F.: Monitoring the Arctic Seas: How Satellite Altimetry Can Be Used to Detect Open Water in Sea-Ice Regions, Remote Sensing, 9, https://doi.org/10.3390/rs9060551, 2017.

Passaro, M., Kildegaard, S. R., Andersen, O. B., Boergens, E., Calafat, F. M., Dettmering, D., and Benveniste, J.: ALES+: Adapting a homogenous ocean retracker for satellite altimetry to sea ice leads, coastal and inland waters, Remote Sensing of Environment, https://doi.org/10.1016/j.rse.2018.02.074, 2018.

Preisendorfer, R. W.: Principal component analysis in meteorology and oceanography, Amsterdam ; New York : Elsevier ; New York, NY, U.S.A. : Distributors for the U.S. and Canada, Elsevier Science Pub. Co., 1988.

Pujol, M. I. and Mertz, F.: PRODUCT USER MANUAL For Sea Level SLA products, GLOBAL OCEAN GRIDDED L4 SEA SURFACE HEIGHTS AND DERIVED VARIABLES REPROCESSED (1993-ONGOING), 1.0, http://resources.marine.copernicus.eu/?option=com_csw&view=details&product_id=SEALEVEL_GLO_PHY_L4_REP_OBSERVATIONS_008_047, CMEMS Product ID: $SEALEVEL_GLO_PHY_L4_REP_OBSERVATIONS$_008_047, 2019.

Rascle, N. and Ardhuin, F.: A global wave parameter database for geophysical applications. Part 2: Model validation with improved source term parameterization, Ocean Modelling, 70, 174 – 188, https://doi.org/10.1016/j.ocemod.2012.12.001, ocean Surface Waves, 2013.

Ray, R. D. and Douglas, B. C.: Experiments in reconstructing twentieth-century sea levels, Progress in Oceanography, 91, 496 – 515, https://doi.org/10.1016/j.pocean.2011.07.021, 2011.

Ringler, T., Petersen, M., Higdon, R. L., Jacobsen, D., Jones, P. W., and Maltrud, M.: A multi-resolution approach to global ocean modeling, Ocean Modelling, 69, 211 – 232, https://doi.org/10.1016/j.ocemod.2013.04.010, 2013.

Rio, M.-H. and Etienne, H.: Copernicus in situ TAC, Global ocean delayed mode currents from drifting buoys, Product User Manual - PUM, Report (technical document (specification, manual)), https://doi.org/10.13155/41257, CMEMS Product ID: $INSITU\_GLO\_UV\_REP\_OBSERVATIONS\_013\_044$, 2018.

Rio, M.-H. and Hernandez, F.: High-frequency response of wind-driven currents measured by drifting buoys and altimetry over the world ocean, Journal of Geophysical Research: Oceans, 108, https://doi.org/10.1029/2002JC001655, 2003.

Rio, M.-H., Mulet, S., and Picot, N.: Beyond GOCE for the ocean circulation estimate: Synergetic use of altimetry, gravimetry, and in situ data provides new insight into geostrophic and Ekman currents, Geophysical Research Letters, 41, 8918–8925, https://doi.org/10.1002/2014GL061773, 2014.

Rudels, B.: Arctic Ocean circulation and variability - advection and external forcing encounter constraints and local processes, Ocean Science, 8, 261–286, https://doi.org/10.5194/os-8-261-2012, 2012.

Schaffer, J., Timmermann, R., Arndt, J. E., Kristensen, S. S., Mayer, C., Morlighem, M., and Steinhage, D.: A global high-resolution data set of ice sheet topography, cavity geometry and ocean bathymetry, Earth System Science Data Discussions, 2016, 1–21, https://doi.org/10.5194/essd-2016-3, 2016.

Volkov, D. L. and Pujol, M.: Quality assessment of a satellite altimetry data product in the Nordic, Barents, and Kara seas, Journal of Geophysical Research: Oceans, 117, https://doi.org/10.1029/2011JC007557, 2012.

Wang, Q., Danilov, S., Sidorenko, D., Timmermann, R., Wekerle, C., Wang, X., Jung, T., and Schröter, J.: The Finite Element Sea Ice-Ocean Model (FESOM) v.1.4: formulation of an ocean general circulation model, Geosci. Model Dev., 7, 663–693, https://doi.org/10.5194/gmd-7-663-2014, 2014.

Wekerle, C., Wang, Q., von Appen, W.-J., Danilov, S., Schourup-Kristensen, V., and Jung, T.: Eddy-Resolving Simulation of the Atlantic Water Circulation in the Fram Strait With Focus on the Seasonal Cycle, J. Geophys. Res. Oceans, https://doi.org/10.1002/2017JC012974, 2017.

Anonymous Referee #1 Received and published: 10 September 2019

We thank the Reviewer for the careful and constructive comments. The suggestions and corrections have greatly improved the quality of this manuscript.

1 General comments

The article describe a new dataset constructed using altimetry, along-track measurements with the outputs a high-resolution numerical model in the "northern Nordic Seas". Overall the article is clearly written and all the details concerning the processing is provided. Nevertheless I formulate 3 main comments regarding the present version of the manuscript:

1. The innovation: the manuscript would be enriched if the authors add a brief justification of the advantages of their new dataset with respect to results of numerical simulations in the same area.

When combining observation data with model simulations we combine and capitalize the advantages of both datasets and get rid of their individual disadvantages. Numerical simulations (without data assimilation) rely on the underlying mathematical/physical relations, which are in all cases simplifications of reality based on specific assumptions. In contrast, observations capture the reality. However, they suffer from measurement errors and sparse spatial resolution. In our study, we mainly rely on the observational side and fill data gaps by model simulations. It's not our intention to compete with ocean models, but to improve altimetry derived datasets. In the manuscript, we showed that the combined dataset has a lot of advantages with respect to satellite only solutions (see comparison with ADT).

We theoretically discuss the differences between models and observations in the introduction, especially in line 10 to 18 on page 3. We add some more information in the introduction on this. A performance comparison between FESOM and combined data is not in the focus of the paper.

We added the following text passage to the manuscript P2 L31:

„Besides observation-based ocean circulation products, model simulations provide information about the ocean dynamics. ***In general, their resolution is much better than these of observations, however, they rely on the underlying mathematical or physical formulations, which naturally contain simplifications and suffer from deficiencies in process descriptions.*** Ocean models differ in spatio-temporal resolutions, forcing model background and underlying mathematical formulations. Recent developments are focusing on so-called unstructured ocean models…"

2. The dataset itself: while it is clear that the FESOM model is based on finite elements, having the different variables on such an unstructured grid may not be the easiest option for most of the users.

We agree with the Reviewer and added a python code to the datastorage (PANGAEA) for an easy regridding of the combined dataset. Please also see section 3 “Comments on data files”.

3. The notations: starting from the schema (Figure 3), the way the different variables are defined make the developments difficult to follow. Suggestions are provided in the specific comments. I believe that the overall quality and the readability would be improved if the authors can address these 3 points.

We agree with the Reviewer and changed the naming of the variables. Please see section 2 “Specific comments”.

2 Specific comments

P1 L9: it is stated that the presented method differs from data assimilation because it substitutes altimetry data with the model output; however it is not clear in the manuscript what is the advantage over the dataset obtained with a pure assimilation approach.

Data assimilation is a completely different combination strategy. Of course, it would be interesting to compare both combination approaches, however, no assimilated FESOM version is available for such comparison, and it is beyond the scope of this paper, to create such a model. Moreover, we do not claim that our approach outperforms an assimilation approach. Our product is mainly focused on the observational side by filling in modeled DOT elevations, where altimetry data is missing or corrupted. This is already stated in the manuscript (page 3, line 14/15).

P1 L14: the by altimetry obtained annual signal→the annual signal obtained by altimetry

We changed the text, accordingly.

P1 L17: and the temporal variability of the altimetry along-track derived DOT heights→specify the temporal resolution (1 day according to the netCDF)

In fact, the temporal resolution of satellite altimetry depends on the repeat cycle of the used mission. What is meant is the high along-track (spatial) resolution (20 Hz measurements). Thanks for pointing out that this sentence is misleading. We replaced it by:
The resulting final product exploits the advantages of both input data sets combining the accurate high-frequent along-track altimetry observations with the high spatial resolution of the ocean model. It is provided with daily resolution on the original FESOM grid.

P1 L21: what justifies the difference in the order of magnitude (0.004 vs 0.02 m/s) for the zonal and meridional components?

The study area is characterized by currents with a predominantly meridional flow direction (e.g. East Greenland Current, West Spitsbergen Current). Due to this reason,

the meridional signal shows a stronger magnitude and variance resulting in bigger differences in the v-component (north-south direction). Please also find P 13 Line 13 and the new added map (Figure 1) showing the major current systems in the investigation area.

P2 L1: drifter location interpolated combined geostrophic velocity components→combined geostrophic velocity components interpolated onto the drifter locations

We changed the text, accordingly.

P2 L2: a general map with the main geographical features would help the readers unfamiliar with the region of interest.

We added a map including the major bathymetric features and major current systems.

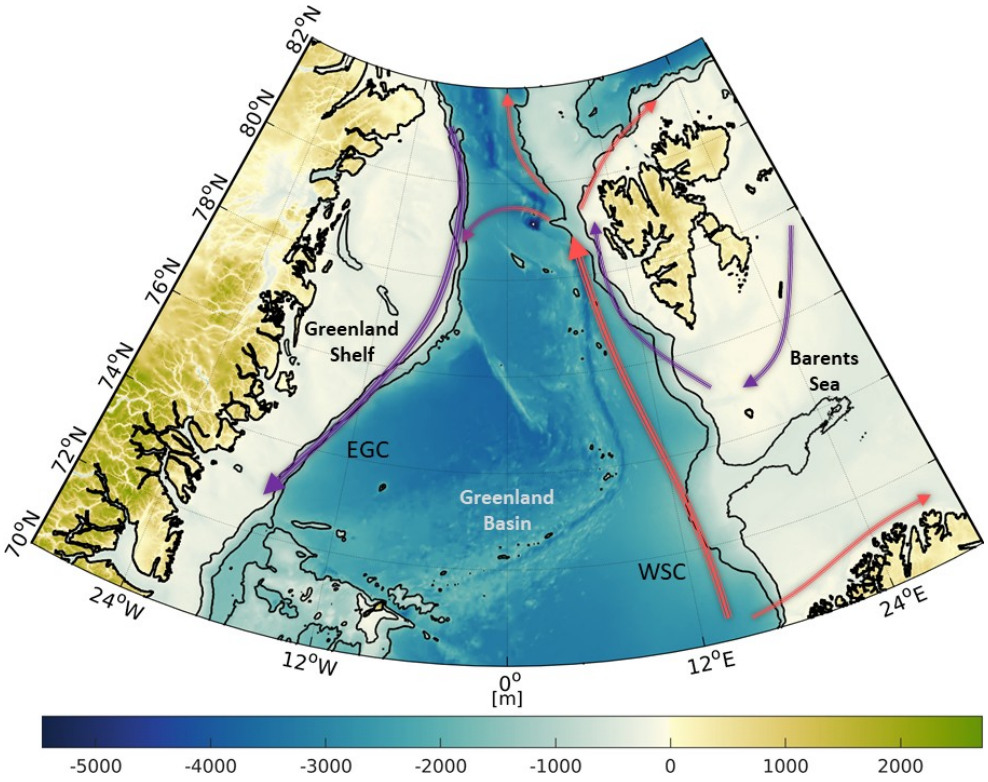

Bathymetry of the study area (norhern Nordic Seas, Fram Strait) based on RTopo2 topography model (Schaffer et al. 2016). Major current systems (West-Spitsbergen Current, WSC; East Greenland Current, EGC) are displayed by arrows in red (inflowing Atlantic water) and blue (returning polar water). Contour lines indicate depths of -450 and -1500 meters.

P2 L18: by altimetry derived geostrophic ocean currents→geostrophic ocean currents derived by altimetry or altimetry-derived geostrophic ocean currents

We changed the text, accordingly.

[...] ***geostrophic ocean currents derived by altimetry*** *suffer from [...]*

P2 L29: CMEMS stands for "Copernicus Marine Environment Monitoring Service"

We apologize for the wrong abbreviation and change the text, accordingly

P2 L32: and underlying mathematical functions→mathematical formulations

We changed the text, accordingly.

P2 L31: information of the ocean dynamics→information on/about the ocean dynamics

We changed the text, accordingly.

P3 L2: about the FESOM model→indicate the version of the code and maybe a DOI referring to that version

We added some information to the text. Please also note section 7 “Data availability”, where we provide a data link including a DOI and a link to the model code. For an easier readability, we use the abbreviation FESOM instead of FESOMv1.4.

New text: *Recent developments* ***focus*** *on so-called unstructured ocean models, allowing for locally highly refined spatial resolutions (Danilov, (2013)), while keeping a coarser resolution in other regions of the Earth* ***(e.g. Finite Element Sea ice Ocean Model, Wang et al, (2014) or Model for Prediction Across Scale Ocean model (MPAS-Ocean), Ringler et al. (2013)). One of the unstructured models is the Finite Element Sea ice Ocean Model version 1.4 (FESOMv1.4) described by Wang et al. (2014)). Please note, in the following text FESOMv1.4 is abbreviated by FESOM.***

P3 L25: the regional extent could be added on a map with the main features (see previous comment)

Please see above, we added a map to the article.

P3 L33: there are other satellites available during that period, why not use them?

In the present article, we use only radar altimetry missions completely covering the investigation area. This prevents the usage of CNES/NASA missions (TOPEX/Poseidon, Jason-1, 2) and NOAA mission GEOSAT Follow-On showing an orbit inclination of about 66 degrees and ~72 degrees. Furthermore, the altimetry data preprocessing (i.e the unsupervised classification approach and the radar waveform retracking algorithm, ALES+) is only applicable to pulse-limited satellite altimetry missions. This limits the available missions to ERS and Envisat. However, in future it should be possible to extend the classification and retracking approach to Delay-Doppler (SAR) altimetry missions (CryoSat-2, Sentinel-3A/B). Please see also chapter 6, Summary and Conclusions.

P4 L1: The data pre-processing from ERS-2 and Envisat observed ranges to derived DOT heights and follows the descriptions of Müller et al. (2019).→it seems a verb is missing

We follow the Reviewer's comment and changed the sentence. It seems the „and" is at a wrong place.

The data pre-processing from ERS-2 and Envisat observed ranges to derived DOT heights ~~and~~ follows the descriptions of Müller et al. (2019).

P4 L4: high resolved and with in-situ data combined→high resolution and combined with in-situ data

We changed the text, accordingly.

P4 L7-8: The manuscript refers to several of the altimetric variables (SSH, SLA, DOT,DWH, ADT, . . .) and it would make the reading easier of the mathematical relationships between them was indicated.

We follow the Reviewer's suggestion and added a list of abbreviations and nomenclature of altimetry as well as FESOM related variables. Please see Appendix A.

P5 Figure 2: Figs 1 and 2 could be merged into a single one where the dots of Fig. 1 are overlayed on Fig. 2 with a common colorbar. Doing so, the comparison would be straightforward and the offset mentioned in the figure caption more obvious.

Figure 1 and Figure 2 should just show the input datasets (altimetry and model) before the combination process. The main point here is the different spatial data distribution. The offset, which has already discussed in detail in Müller et al. 2019 is only of minor interest (as it is reduced before the combination). We think the combination of both plots would make it difficult to see the satellite tracks, since the FESOM representation will dominate the along-track data of altimetry. We decided to change the caption of Figure 2.

Note the offset in comparison to Figure 1 → Note the different scaling of colorbars in comparison to Figure 1.

P5 L8-9: for traceability purpose, indicate the product number from the CMEMS catalog.

We added the product number to the references.

P5 L9: same comment concerning the meaning of CMEMS acronym.
We thank the Reviewer and changed the text, accordingly.

P5 L17: must be corrected enabling→must be corrected in order to enable

We changed the text, accordingly.

P6 L30: define 'differential water height" (see previous comment concerning the different altimetric variables).

Please see Appendix A and previous comment.

P7 Fig. 3: what is the relation between DOT and DWH?

Please see chapter 2.2 and for further explanations the publication of Androsov et al., 2018. DWH are differential water heights with respect to a virtual defined reference surface. In case of FESOM DWH are very similar to DOT heights, however secular changes like gravitational forces or the Glacial Isostatic Adjustment (GIA) are not considered. Following the explanations of Androsov et al. (2018) the volume conservation of FESOM leads to correct modeled horizontal gradients but to a constant offset (~47cm) between the simulated heights and the geodetic by altimetry derived DOT. Moreover, the offset can be also confirmed in Müller et al. (2019).

Androsov, A., Nerger, L., Schnur, R., Schröter, J., Albertella, A., Rummel, R., Savcenko, R., Bosch, W., Skachko, S., and Danilov, S.: On the assimilation of absolute geodetic dynamic topography in a global ocean model: impact on the deep ocean state, Journal of Geodesy, https://doi.org/10.1007/s00190-018-1151-1, 2018.

Müller, F. L., Wekerle, C., Dettmering, D., Passaro, M., Bosch, W., and Seitz, F.: Dynamic ocean topography of the northern Nordic seas: a comparison between satellite altimetry and ocean modeling, The Cryosphere, 13, 611–626, https://doi.org/10.5194/tc-13-611-2019, 2019

The colors don't really improve the readability of the flow charts: it seems clear that the altimetric data and the FESOM simulations are the 2 inputs and that blue boxes represent combination (since they receive information from 2 other boxes).

We decided to keep the different colors. Even if their definition might be obvious, their usage will not degrade the readability of the plot. However, we agree to unify the colors of the input datasets. Plot and caption have been updated.

The choice of having uppercase for the variables defined on the grid and lowercase for the along-track variables is maybe not necessary, since you write $coord_{obs}$ or $coords_{sim}$ before the variable name.
The variable names could conserve the same name (with uppercase) but then the spatial coordinates could be X, Y for the grid and x, y for the along-track measurements. Doing so, one avoids the use of $coord_{sim}$ and $coord_{obs}$.

We follow the Reviewer's suggestions and change the labeling of the various coordinate representations. Please also note the changed caption of Figure 3 (processing scheme).

P8 L8-16: for the determination of the number of modes that will be conserved, there is not a real justification. Instead of selecting 50 modes and then computing the resulting RMSE, another approach could be: select the minimal number of modes than ensure that the RMSE is below a given threshold. Figure 4 tends to show that the higher-order modes almost don't contribute to the variance.

We agree with the Reviewer's opinion. Maybe the sentence is misleading. Our goal is to ensure a 10 mm error budget in the pure reconstruction of FESOM. Thus, we tested how many modes are needed to reach this 10 mm error in maximum. The Reviewer is absolutely correct by explaining that higher-order Modes don't contribute to the total variance. We also wanted to show this in Figure 4.

We changed the sentence: ***It is decided to use a RMSE threshold of 10mm, corresponding to 50 Modes and a summed variance of more than 99%.***

P9 Eq. 2: similarly to other comments: the notations can be improved, for instance avoiding using 3 subscripts (pc_{combi}). Why not something like $P_i(t)$instead (for example)?

We follow the Reviewer's suggestions and change the labeling. Please also note the changed caption of Figure 3 (processing scheme).

P9 L21: interpolated to observation coordinates→which interpolation method is used?

We used a simple nearest neighbor interpolation. We added further information to the text.

*The individual weights are defined by using external sea ice concentration from the National Snow and Ice Data Center (NSIDC, Fetterer et al. (2017)) interpolated v**ia nearest-neighbor interpolation** to the observation coordinates **considering** an [...]*

P10 Fig. 5: this figure could be discarded easily by adding the numbers (1-4) to Figure3.

We agree with the Reviewer since Figure 5 is a zoom of Figure 3, however, we want to highlight the key stages (1-4) of the combination process. We think it's easier to understand for readers, who are no experts in PCA to follow the different processing stages step by step.

P11 L3: which prevents further smoothing effects→please explain shortly why the finite element method prevents this.

The benefit of computing geostrophic currents via finite element methods can be seen in a direct derivation on the grid nodes without an additional interpolation. Normally, an inclined plane is fitted to the grid nodes computing zonal and meridional slope coefficients. Therefore, neighboring height values must be interpolated using a certain cap size, which causes smoothing and damping effects.

We changed the text to: "… which prevents further smoothing effects, **since no re-gridding to a regular grid is necessary**."

P11 L5: Comparison with external datasets→couldn't you consider a comparison with the altimetric measurements acquired by the satellites not used in this study?

We agree with the Reviewer that it is a good idea to use altimetry data, which is not part of the study as validation data. However, currently, there is no altimetry data we can use, which is consistent with the observations used for the product generation. Our algorithms are valid for pulse-limited, i.e. conventional satellite altimetry missions. This holds for the classification approach as well as for the retracking of the radar echoes. Delay-Doppler missions, such as CryoSat-2 are based on another observing principle resulting in different radar echoes. ALES+, the physical retracker used in the present study is not applicable to Delay-Doppler data. Thus, a fair and consistent comparison or validation is currently not possible with this mission.
Moreover, radar altimetry data from CNES/NASA missions TOPEX/Poseidon, Jason-1,2, 3 and NOAA mission GEOSAT Follow-On (GFO) can't be used due their limited spatial coverage and orbit characteristics (~66°N/S for Jason-1,2,3 and ~72°N/S for GFO).
In future, it's planned to adapt ALES+ to Delay-Doppler radar echoes in order to include further observed DOT heights to the combination process.

P14 Figure 7: Please note the changed scale of the differences.→the changed range?

We apologize for this wrong caption. There is no changed range. Thank you very much for the comment.

P15 L15: Whereas the obtained spatial resolution is given by FESOM, characterizedby local refinements in ocean current active areas smaller than 1 km.→missing verb (or is part of the previous sentence, then should be separated by a comma).

We changed the sentence to: "the obtained spatial resolution is *defined* by FESOM, *which is* characterized by local refinements…."

P15 L16: Finite Element mesh→sometimes finite element is capitalised, sometimes not, please make uniform.

Thank you for the hint. We uniformed the text (using finite element).

P17 L6: uncompressed FESOM geostrophic currents→define what is the "uncompressed currents".

This sentence was a fragment in the summary/conclusion from a previous version of the article, sorry. The sentence has been deleted now, thank you for the comment.

P17 Data access: the URL relative to ERS-2 points to a news, not to the actual dataset.

We apologize for the wrong link and updated the URL.

New: https://earth.esa.int/web/guest/-/radar-altimeter-reaper-sensor-geophysical-data-record-sgdr

p18 Appendix A: this appendix is rather short and could be included directly in the text,hence ensuring the continuity of the calculations

We thought about this comment and decided to erase Appendix A, because it's a standard procedure and does not contain any special mathematical formulation. More information regarding least-squares can be also found in Koch (1999), which is a standard reference for parameter estimation.

3 Comments on the data files

We really thank the Reviewer for the information about the function "ncatted" and the comments.

Adding the netCDF attributes standard_name for the coordinates (longitude, latitude and time) and for the variables. This does not require a full reprocessing but can be done using for instance the nco operator (http://nco.sourceforge.net/), in particular then catted command allows one to edit the attributes and can be called as:

```
ncatted -O -h -a standard_name,lon,o,c,longitude 1995_NEGO.nc
ncatted -O -h -a standard_name,lat,o,c,latitude 1995_NEGO.nc
```

Concerning the time variable: The long_name is generally specified as "time" and the "units" should be indicate the days (or seconds) since a given date (following the recommendation from the CF conventions: http://cfconventions.org/Data/cf-conventions/cf-conventions-1.7/cf-conventions.html#time-coordinate).

We added "standard_name" to the NetCDF files.

A possible concern is related to the data format: the netCDF is fine and tools are available for reading in many languages, but the finite-element mesh may not be the easiest option for the users, as it may require a regridding. I would suggest to have a similar dataset but provided on a regular grid with a resolution similar to the unstructured grid, or an example (code) of how to go from the unstructured grid to a regular grid.

We decided to provide an example python code, using The Generic Mapping Tools (GMT, http://gmt.soest.hawaii.edu/projects/gmt), for an easy transformation to a regular grid. GMT is a commonly used, well validated open source software and can read directly NetCDF files. A short function description is added to the user manual.

In the Pangaea preview, the map displays 2 markers labeled 1 and 2, but it is not clear what they are. If it is the spatial coverage, a "rectangle" would be more explicit. Also in the Pangaea page, it seems the coverage is not exactly the same as in the netCDF for the longitudes:

Pangaea: South-bound Latitude: 72.000000 * West-bound Longitude: -29.000000 *North-bound Latitude: 82.000000 * East-bound Longitude: 29.000000 netCDF:South-bound Latitude: 72.000000 * West-bound Longitude: -29.803572 *North-bound Latitude: 82.000000 * East-bound Longitude: 29.99896

In case of the overview map we contacted PANGAEA. Unfortunately, it's not possible to add a rectangle for highlighting the study area. We know that a simple Mercator (Google) projection is not the best for polar regions, however PANGAEA does not have any

alternatives. However, the coordinates should be right. We sent a notice to PANGAEA to correct this.

Keywords:the region is specified as "Arctic Ocean" while the article title mentions "the Nordic Seas"

The Keywords are adapted.

Anonymous Referee #2Received and published: 18 September 2019

We thank the Reviewer for the careful and constructive comments. The suggestions and corrections have greatly improved the quality of this manuscript.

The paper describes a new dataset of altimetry and associated geostrophic currents, obtained by merging satellite observations and model simulations, and based on principal component analysis. This approach is a novel way to combine both sources of information and seems to produce consistent results.

I note a certain similarity between this approach and the DINEOF method (see e.g.http://modb.oce.ulg.ac.be/mediawiki/index.php/DINEOF_references) which fills gaps(clouds) in satellite observations using also a PCA method. However in the current paper, the EOFs are obtained from another source of information (a model) than the observations.

Thank you for this link. We were not aware of this method. I fact, this is an interesting method, which is based on EOF as our approach is. However, one big difference is, that we do not use the altimetry observations for EOF analysis, since they are not available in fixed locations and with uniform epochs. In contrast, we use external data (a model) in order to fill the data gaps. That's why we decided not to mention DINEOF in the introduction of our manuscript.

The authors have carefully addressed the preprocessing required to merge the 2 datasets (offsets etc). The dataset itself is easy to download and read (at least for users with experience of netcdf files, which is standard). Given each file is large (~2 GB), users who wish to download the entire dataset would maybe appreciate compressed netcdf files. Most services are switching to netcdf4 compressed files (e.g. CMEMS).

We follow the Reviewer's suggestion and compress the NetCDF files with the highest compression level, which results in a total reduction of about 14GB.

The paper is well written, generally clear and generally does not contain typos. I only have a few general comments or requests for clarifications. In the remainder of the review, by "dataset" I mean the new product that readers can download.

* page 2 line 7-11. The mentioned regions and main currents should be indicated on a map (e.g. Fig 2 that could then be moved higher in the text).

We follow the Reviewer's suggestion and added a map containing major currents and bathymetric features to the introduction (see new Figure 1)

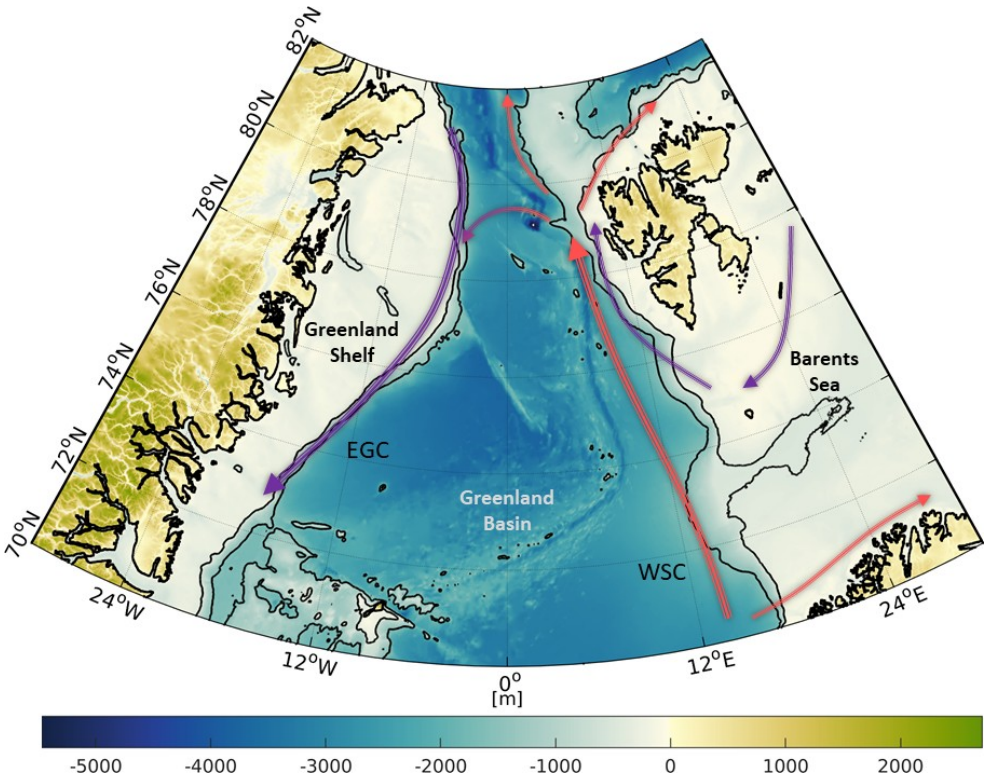

Bathymetry of the study area (norhern Nordic Seas, Fram Strait) based on RTopo2 topography model (Schaffer et al. 2016). Major current systems (West-Spitsbergen Current, WSC; East Greenland Current, EGC) are displayed by arrows in red (inflowing Atlantic water) and blue (returning polar water). Contour lines indicate depths of -450 and -1500 meters.

* page 9 line 12: write out NN. Only on a later page do we learn it means nearest neighbour (page 10 line 1)

We changed the text, accordingly.

* page 9 line 25 : it is not clear why the the description of the "individual steps" is provided separately. For example what is written on page 9 line 27-28, has already been mentioned explicitly before (page 8 line 15). Also the corresponding figure (5) is useless as it is just a zoom on a previous figure

You are right that the list of individual combination steps is redundant information. The intention is to highlight the key processing steps in order to make it easy for the readers to understand the procedure. We think that the Figure is helpful for other, less experienced readers and decided to keep the figure and explanations.

* page 11 line 9-10: "contain" is misleading. Reading this, I could have the impression that the dataset contains the 2 things (satellite & model). By now, the reader has understood that the dataset is build using the 2 sources, but it (i.e. the netcdf file) does not "contain" them. Please rephrase.

We agree and changed the text, accordingly.

The combined DOT and geostrophic current velocity fields are based on DOT heights from satellite altimetry [...].

* page 11 line 15: the fact that outliers in the results are rejected, has not been mentioned in the method description. We learn only now about it.

We agree and added some text to section 3.2. (step 4). Text passages in chapter 4 are now redundant and deleted.

New text chapter 3.2 (P 10 Line 5) :

Furthermore, an outlier detection based on an accuracy determination of the combined principal components is performed to reject erroneous combination estimations.

Deleted text chapter 4: (P 11 Line 15):

Furthermore, an outlier detection based on the accuracy of the computed combined principal components is performed rejecting erroneous combination estimations.

* figure 6, right column. Wouldn't a quiver plot (arrows) be more explicit than the colors for indicating the direction?

We tried quiver plots for displaying the flow direction. However, the unstructured grid is very dense (~1km), resulting in a lot of arrows reducing the readability. Therefore we decided to indicate the flow direction by using a circular phase map ranging from [-180° to 180°].

* pages 11,13-15 : the authors compare the dataset with different other sources of DOT and currents: "processed" drifter data, original drifter data, ADT. About the second comparison, page 13 lines 16-19, please specify if the rmse computed directly between the drifter and the dataset, is taking as input the original drifter velocity, or is preprocessed (e.g. taking into account only the geostrophic part). Also, line 17, how come the RMSE is suddenly large (0.13 m/s) in this case, especially compared to the velocity itself?

We apologize for the confusion. We only use "processed" drifter data, which means only the geostrophic part of the drifter total velocity. We use a 6 hourly interpolated drifter dataset and reduce the individual observations by a-geostrophic (wind, wave) movements. In this second comparison, we directly compare the geostrophic drifter trajectories, which means the single geostrophic drifter observations, with the combination velocities. The numbers are higher than for the gridded comparison, because the individual drifter trajectories are characterized by a high noise budget and a strong variability.

Change text to P13 L16: *When computing the RMSE between the measured geostrophic velocities and the combined velocities based on the individual trajectories for each drifter, a mean of…*

Finally, apart from the comparisons proposed in the paper, would it make sense to compare the dataset with the DOT obtained directly from FESOM? In a perfect world, the

dataset would even be compared with a data-assimilating version of FESOM, but I understand this is a whole new work and out of the scope of the article.

We don't think that a comparison of the new product with the original FESOM model is able to provide new findings. Of course, differences will exist, but the observations will not improve the model (for this purpose a data assimilation or calibration would be required, which keeps the model physics). This was not the aim of the study. We want to improve observation-based velocities, that's why we only include comparisons to observation-only products.

* page 17 line 6 : the comparison between "uncompressed" FESOM geostrophic cur-rents and the dataset : what is the meaning of uncompressed? Also in the article itself, please indicate clearly where you compared the pure FESOM outputs with the dataset, leading up to this phrase in the conclusion.

This sentence has been deleted, since it was wrong. There is no comparison between FESOM and the combined dataset.